Response to Anonymous Reviewer #1

We thank anonymous referee #1 for their helpful comments on this work. Below, original comments are in italics and our responses are in bold.

General comments:

Although the paper is generally well-structured, it does appear to jump around a bit when describing the various tests that were carried-out. For example, at the beginning of section 5 (P5378), it would be helpful to include a list of the types of tests (in addition to Table 3), or at least just mention that there are also tests considering temporally varying errors in the prior parameters. Another point that I found confusing was whether or not transport (and measurement) errors were added to the pseudo-observations, as the impact of these is mentioned later in section 5.2 (P5383).

We have added some text at the beginning of Section 5 to mention that a temporally-varying bias is considered for some of the tests. We have also added a sentence indicating which tests can be found in which subsection of Section 5. We did not add random noise to the pseudo observations in most of these tests, but did perform a subset of tests with noise added that yielded the same results as the tests with no noise. We have added some text to mention this.

Specific comments:

P5370, L20: please change this to: "Agricultural activities such as fertilizer application and animal waste management increase the substrate available for nitrification and denitrification pathways leading to enhanced..." as by writing that the reactions are enhanced suggests increased rates of reaction.

We have made this change.

P5371, L5-8: suggest that the authors also include reactive nitrogen substrate in this list, as it is one of the most important determinants of N2O emissions

We have made the addition to the list.

P5374, L8: by "loss frequencies" do the authors mean photolysis cross-sections or other, please clarify.

By loss frequencies we mean the loss due to both photolysis and reaction with $O(^1D)$. We have added some text to clarify this.

P5375, L23: by enforcing a minimum value of the posterior scaling parameters of zero implies that the fluxes cannot change sign in the inversion, i.e., a negative flux cannot become positive and vice-versa. Is this what the authors mean? In which case it is not quite correct that regions with a prior negative flux (e.g. over the ocean) cannot become more negative, but rather that they cannot become sources?

Correct—we thank the reviewer for catching that. We have updated the text to note that the assumption implies that the sign of the a priori N_2O flux is correct (i.e. net sinks will remain net sinks and vice versa).

P5375, L19: does the size of the state vector apply to the two-year inversion period? Given that the number of elements for the stratospheric loss parameters is 192, I would be presume so, but it would be helpful to state this here.

Yes. We have added some text to note that the state vector corresponds to the two-year inversion.

P5376, L6: could you please give the order of magnitude of the transport errors calculated? This would be interesting to know, especially in connection to the influence of the transport errors on the ability for the inversion to simultaneously optimize the emission and loss parameters.

The transport errors are quite small at the surface (0.2 ppb on average), but can be much larger aloft when calculated with respect to an aircraft's location (2-8 ppb on average). We have added some text to include this information.

P5378, L23: do you add any random noise to the pseudo-observations, and if so, was this consistent with the error characteristics of the observation error covariance matrix?

The tests presented here do not have random noise added to the pseudo observations, but we did do a subset of tests in which we added random noise (consistent with the observation error, which is the sum of measurement and model transport error) and got the same results as the tests with no random noise. We have added some text to note this at the beginning of Section 5.

P5378, section 5: by adding a spatially uniform error to the prior values of the scaling parameters, you are testing the ability of the inversion to correct a uniform bias, which effectively means one degree of freedom. However, it would be also a useful test to see how well random spatially distributed errors can be corrected.

We did perform a test in which we assimilated surface pseudo observations and applied a spatially-random emission bias of up to ±50%. The correction to the random bias was slight, and occurred mainly in the vicinity of sites with continuous observations. We opted not to include this test as the error reduction calculations give the same information. We have added a sentence to Section 5.4 mentioning this.

P5380, L1-5: did the authors examine how the correction to the biased a priori scaling factor varied from season to season? I would expect that there would be some dependency on season as well due to the seasonal variation stratosphere-to-troposphere (STT) mixing on the tropospheric mixing ratios of N2O. This would be useful information to include.

For the case of a uniform bias in emissions, the correction to the scaling factor has very little variation month-to-month. The only variability appears to be due to the temporal variability of emissions in the a priori database for ocean emissions.

P5382, L5-10: I think here it is important that the authors make a distinction between the lower and upper stratosphere. The vast majority of the loss of N2O occurs in the upper stratosphere, therefore, the influence of a bias in the loss will only be seen in the troposphere (where the nearly all the observations are made) after the time delay for transport from the upper stratosphere to the troposphere, which is long, i.e. 1-2 years. However, mixing from the lower stratosphere to the troposphere can occur on shorter timescales of weeks to months.

This is a good point. We have added some text to make the distinction that the timescale of mixing from the upper stratosphere to the troposphere is what drives the ability to correct the biased a priori values.

P5394, L1: although in the future, satellite retrievals of N2O may reach the precision and accuracy needed to help constrain N2O emissions, current retrievals and instruments are not at this level: the error on N2O retrieved from AIRS is about 7 ppb in the troposphere (for comparison, this is more than 3 times the inter-hemispheric gradient in N2O). At present, the AIRS satellite retrieved may be helpful in addition to ground-based observations for, e.g., establishing the vertical profile of N2O for the initial conditions but not in solving for surface emissions of N2O.

We agree with this statement and have expanded this point in the Conclusions.

Technical comments:

P5369, L8: replace "aboard" with "on-board", i.e., the adjective

We have made this change.

P5370, L13: 100-year

We have made this change.

P5370, L15: "those of any other ozone depleting substance"

We have made this change.

P5370, L16: replace "reactions" with "pathways" as nitrification and denitrification each involve a series of reactions

We have deleted "reactions".

P5375, L23: "...ocean regions with a net N2O uptake are not stronger sinks than in the prior..."

We have altered the text here to address the specific comment above.

P5377, L25: please put the phrase in brackets "(in general...)" after "lowermost stratosphere" to make the sentence easier to understand

We have made this change.

Response to Anonymous Reviewer #2

We thank anonymous referee #2 for their helpful comments on this work. Below, original comments are in italics and our responses are in bold.

P5370, lines 2-4: the sentence about averaging kernels seems a bit technical and out of place in the abstract, I think it would be beneficial for the reader to change this description to say something about the inversion sensitivity to the emissions.

We have added a definition of the averaging kernel in the abstract as well as in Section 5.4.

P5370, lines 12:15: I think the first two sentences would read better if merged into a single sentence

We prefer to keep this as two sentences, but have included the word "also" in the second sentence to improve the flow.

P5371, line 28: suggest changing "scale on which" to "scale over which"

We have made this change.

P5372, line 25: it would be useful to have a brief description of CARIBIC, including a definition of the acronym, on the previous page as is done for HIPPO. Would it also be useful to reference any previous studies of the CARIBIC N2O?

We have added a definition of the acronym here. Previous studies by Schuck et al. and Assonov et al. are cited later in Section 4.

P 5373, line 11: suggest moving GEOS-5 to go after the definition.

We have made this change.

P5373, line 12: clarify longitude and latitude for horizontal resolution?

We have made this change.

P5373, line 16: suggest using "anthropogenic" rather than "anthropogenic sources"

We have made this change.

P5374, line 9: define what MERRA means.

We have made this change.

P5374, Section 4: it might be useful to include a short paragraph on satellite observations of N2O either at the end of this section or in the introduction, especially as this is very briefly touched on at the end of the summary section.

Because we do not include any satellite-based observations of tropospheric N_2O in this study, we prefer not to include a paragraph describing them in the methods section. While there has been recent work developing tropospheric N_2O retrievals from satellite-based infrared sounders (such as the AIRS retrieval mentioned in the summary), these are currently not validated or publicly available.

P5379, line 7: suggest changing "based on" to "using"

We have made this change.

P5381, lines 1-7: it would be useful if the authors could comment on the sensitivity of the inversion to the vertical profile of the measurements here – it looks to me as though the HIPPO observations provide a stronger constraint because they extend throughout the troposphere to the surface, therefore, do the authors have any sense as to the altitude range at which the constraint breaks down? This would be especially useful in the context of Section 5.5 and would maybe make a strong statement on the importance of in situ profiles from aircraft as part of the global observing system.

This is a good point. We have added some text to mention that the HIPPO observations include profiling from the boundary layer to the upper troposphere, which is likely the major reason why it provides a stronger constraint than CARIBIC. Additionally, we point the reviewer to the error reduction results in Figure 9, which show that significant

error reduction is achieved with CARIBIC only in the vicinity of Frankfurt where flights in the lower troposphere occurred.

P5381, line 23: should "sources as well as sinks" be "sinks as well as sources"? the previous subsection has dealt with sources and this one talks more about the sink.

We have made this change.

P5382, line 7: stating that the second year is the final year seems a bit unnecessary, also the statement that "the inversion does not significantly affect the observations" seems to be the wrong way around to me – isn't it the impact of the observations on the inversion which is being assessed?

We choose to keep the statement that the second year is the final year as a reminder to readers. We have reworded the latter statement as we agree it was confusing as is. We have changed the text to say "Stratospheric loss of N_2O in the second (i.e. final) year of the inversion does not significantly affect the N_2O mixing ratios at the observation locations" meaning that biased stratospheric loss will not have a measurable signal in the troposphere during the second year of a two-year simulation. Because of this the (pseudo) observed mixing ratio and model mixing ratios are very similar, and there is insufficient forcing to correct a prior bias.

P5383, line 1: it's hard to tell from the Figure that there is any significant change in the a posteriori compared to the a priori.

The changes between a priori and a posteriori in the right-hand panels of the figure are indeed very subtle. We have zoomed in the y-axis range to try to address this (from 0 to 1.5 instead of 0 to 2) and also added some text to note that the deviation from the a priori is very slight.

P5383, lines 24-26: it would be useful if the authors could comment here on any vertical correlations that might help to address this, or which limit the impact of aircraft observations measured at cruise altitude

We have made this addition.

P5385, lines 1-2: it might be useful if the authors could comment briefly on how the box model results relate to transport across the tropopause on different timescales (e.g. tropical vertical mixing vs. isentropic mixing in the extratropics)

The disclaimer on P5384, lines 5-7 indicates that the box model results do not capture seasonal effects or spatial gradients within the stratosphere/troposphere. It would also not capture stratosphere-troposphere transport mechanisms that occur on different timescales. We have added this to the text.

6

P5386, line 2 and P5387, line 2: please check the consistent use or a priori or prior and a posteriori and posterior.

We have modified the text to include the use of a priori and a posteriori throughout.

P5391, line 25: clarify that the surface observations are both in situ and flask measurements.

We have made this change.

P5392, line 19: is this statement on model transport specific to GEOS-5? It might be useful to add a comment on model transport issues based on other studies using relatively long-lived constituents (e.g. CO2 or CO)

Model transport issues are not specific to GEOS-5. In a TransCom model intercomparison, Thompson et al. (2014, ACP) found the N₂O gradient across the tropopause to vary significantly among eight different chemical transport models, presumably due to differences in modeled vertical transport and rates of strat-trop exchange. We added a citation of that paper at this point in the text.

P5393, lines 5-15: I think that it would be of benefit to the reader if the authors could rephrase the description of the averaging kernels to what it means in terms of the sensitivity of the inversion to the emissions (similar to my comment for the abstract) – by all means this should then reference the averaging kernel values but would be easier to understand the broader significance.

We have added some text to Section 5.4 defining the averaging kernel as the sensitivity of the inversion to emissions in each grid square. However, we feel we have already highlighted the broader significance of the averaging kernel, which is that it tells us about the observational constraints on emissions achieved in a particular location. In instances where the averaging kernel for a location is close to 1.0 at that location and close to 0 everywhere else, the local emissions are well-resolved by the observations in our inversion framework. Conversely, highly smeared averaging kernels indicate that emissions in a particular location are likely to be conflated with those in other parts of the world. This has important implications for how we interpret the inversion results.

P5393, line 13: is it an underconstraint or no constraint in the tropics?

We feel underconstraint is more appropriate than no constraint, because we have only shown rows of the averaging kernel for one tropical location, which does not necessarily mean there is zero constraint throughout the tropics.

P5393, line 21-23: could this also be linked to requirements for similar targeted measurements for other atmospheric constituents, and greenhouse gases in particular? How do the findings here compare to similar studies for CO2 and CH4?

7

Targeted aircraft measurements in the tropics would likely also be useful for any species that has a significant tropical source. N_2O is somewhat unique in that elevated concentrations have been measured aloft in the tropics (e.g. Kort et al., 2011, GRL), indicating the presence of a large, episodic emission source in the vicinity of tropical convection. So, aircraft observation in this region may be particularly useful for N_2O, and would complement the use of surface observations. We have added some text to Section 5.5 to note this.

P5394, line 1: it would be useful to have a brief sentence on satellite observations in the introduction.

As in our response to the similar comment above, we choose not to include any additional information in the introduction since satellite observations are not used in this study.

P5409: clarify that HIPPO or CARIBIC are aircraft measurements.

We have made this change.

Figures 6 and 7 would benefit from some clearer labelling of the plots and reference in the captions.

We have edited the captions for both figures to be more explicit about where the labels are located and which lines refer to which label.

Simulation of atmospheric N_2O with GEOS-Chem and its adjoint: evaluation of observational constraints

K. C. Wells[1], D. B. Millet[1], N. Bousserez[2], D. K. Henze[2], S. Chaliyakunnel[1], T. J. Griffis[1], Y. Luan[1], E. J. Dlugokencky[3], R. G. Prinn[4], S. O'Doherty[5], R. F. Weiss[6], G. S. Dutton[3,7], J. W. Elkins[3], P. B. Krummel[8], R. Langenfelds[8], L. P. Steele[8], E. A. Kort[9], S. C. Wofsy[10], T. Umezawa[11,12]

[1] {Department of Soil, Water, and Climate, University of Minnesota, St. Paul, Minnesota, USA}

[2] {Department of Mechanical Engineering, University of Colorado at Boulder, Boulder, Colorado, USA}

[3] {Earth System Research Laboratory, NOAA, Boulder, Colorado, USA}

[4] {Center for Global Change Science, Massachusetts Institute of Technology, Cambridge, Massachusetts, USA}

[5] {School of Chemistry, University of Bristol, Bristol, UK}

[6] {Scripps Institute of Oceanography, University of California, San Diego, La Jolla, California, USA}

[7] {CIRES, University of Colorado, Boulder, Colorado, USA}

[8] {CSIRO Oceans and Atmosphere Flagship, Aspendale, Victoria, Australia}

[9] {Department of Atmospheric, Oceanic, and Space Sciences, University of Michigan, Ann Arbor, Michigan, USA}

[10] {School of Engineering and Applied Science and Department of Earth and Planetary Sciences, Harvard University, Cambridge, Massachusetts, USA}

[11] {Center for Atmospheric and Oceanic Studies, Tohoku University, Sendai, Japan}

[12] {Max-Planck Institute for Chemistry, Mainz, Germany}

Correspondence to: D. B. Millet (dbm@umn.edu)

1

Abstract

We describe a new 4D-Var inversion framework for N_2O based on the GEOS-Chem chemical transport model and its adjoint, and apply ~~this framework~~it in a series of observing system simulation experiments to assess how well N_2O sources and sinks can be constrained by the current global observing network. The employed measurement ensemble includes approximately weekly and quasi-continuous N_2O measurements (hourly averages used) from several long-term monitoring networks, N_2O measurements collected from discrete air samples on~~a~~board a commercial aircraft (CARIBIC), and quasi-continuous measurements from an airborne pole-to-pole sampling campaign (HIPPO). For a two-year inversion, we find that the surface and HIPPO observations can accurately resolve a uniform bias in emissions during the first year; CARIBIC data provide a somewhat weaker constraint. Variable emission errors are much more difficult to resolve given the long lifetime of N_2O, and major parts of the world lack significant constraints on the seasonal cycle of fluxes. Current observations can largely correct a global bias in the stratospheric sink of N_2O if emissions are known, but do not provide information on the temporal and spatial distribution of the sink. However, for the more realistic scenario where source and sink are both uncertain, we find that simultaneously optimizing both would require unrealistically small errors in model transport. Regardless, a bias in the magnitude of the N_2O sink would not affect the a posteriori N_2O emissions for the two-year timescale used here, given realistic initial conditions, due to the timescale required for stratosphere-troposphere exchange (STE). The same does not apply to model errors in the rate of STE itself, which we show exerts a larger influence on the tropospheric burden of N_2O than does the chemical loss rate over short (< 3 year) timescales. We use a stochastic estimate of the inverse Hessian for the inversion to evaluate the spatial resolution of emission constraints provided by the observations, and find that significant, spatially explicit constraints can be achieved in locations near and immediately upwind of surface measurements and the HIPPO flight tracks; however, these are mostly confined to North America, Europe, and Australia. None of the current observing networks are able to provide significant spatial information on tropical N_2O emissions. There, ~~inversion~~ averaging kernels (describing~~which measure~~ the sensitivity of the inversion ~~in a particular location~~ to emissions in each grid square) ~~are highly smeared spatially and extend even to the midlatitudes, so that

10

tropical emissions risk being conflated with those elsewhere. For global inversions, therefore, the current lack of constraints on the tropics also places an important limit on our ability to understand extratropical emissions. Based on the error reduction statistics from the inverse Hessian, we characterize the atmospheric distribution of unconstrained N_2O, and identify regions in and downwind of South America, Central Africa, and Southeast Asia where new surface or profile measurements would have the most value for reducing present uncertainty in the global N_2O budget.

1   Introduction

Nitrous oxide (N_2O) is a long-lived greenhouse gas with a global warming potential approximately 300 times that of CO_2 on a 100-year timescale (Forster et al., 2007). It is also a key player in stratospheric chemistry; N_2O emissions weighted by their ozone depletion potential currently outrank those of any other ozone depleting substance (Ravishankara et al., 2009). N_2O is produced via microbial nitrification and denitrification reactions pathways in soils (Firestone and Davidson, 1989) and ocean waters (Elkins et al., 1978; Cohen and Gordon, 1979; Law and Owens, 1990), with soils contributing the majority of the global flux (Mosier et al., 1998). Agricultural activities such as fertilizer application and animal waste management enhance these nitrification and denitrification reactions increase the substrate available for nitrification and denitrification pathways (Maggiotto et al., 2000), leading to enhanced direct on-site emissions as well as indirect emissions downstream due to leaching and runoff (IPCC, 2006). Energy production and transportation (Denman et al., 2007) and biomass burning emissions (van der Werf et al., 2010) also contribute to the global N_2O source. N_2O is lost in the stratosphere via photolysis and reaction with $O(^1D)$, leading to a global lifetime currently estimated at ~122-131 years (Volk et al., 1997; Prather et al., 2012). Atmospheric N_2O is currently increasing at ~0.8 ppb yr^{-1} (http://ds.data.jma.go.jp/gmd/wdcgg/pub/global/globalmean.html), driven by accelerating human perturbation of the nitrogen cycle: in particular, rising application of nitrogen fertilizers (Galloway et al., 2008; Davidson, 2009; Park et al., 2012) and the nonlinear response of soil N_2O emissions to N fertilizer inputs in excess of crop demands (Shcherbak et al., 2014).

1   Rates of microbial nitrification and denitrification in soils depend strongly on environmental

2   characteristics such as temperature (Potter et al., 1996), moisture (Bouwman, 1998; Bouwman

3   et al., 2013), availability of reactive nitrogen substrate, and the make-up of the soil microbial

4   community (Butterbach-Bahl et al., 2013), and as a result large uncertainties exist in the

5   spatial and temporal distribution of global N_2O emissions. Long-term flask-based and in-situ

6   observations of atmospheric N_2O are available from a number of monitoring networks around

7   the world, along with routine and intensive aircraft observations, and there have been several

8   recent studies employing these data to generate top-down estimates of global N_2O emissions.

9   Huang et al. (2008) derived a global N_2O flux of 14.1-17.1 Tg N yr^{-1} for 2002-2005 using

10   surface observations from four different surface monitoring networks. Based on aircraft

11   observations from the first two HIAPER Pole-to-Pole Observations (HIPPO) campaigns, Kort

12   et al. (2011) found evidence for large and episodic tropical fluxes. Saikawa et al. (2014)

13   combined surface observations with aircraft- and ship-based measurements to derive regional

14   N_2O emission estimates for five source sectors, and inferred a global flux of 18.1 ± 0.6 Tg N

15   yr^{-1} for 2002-2005. Thompson et al. (2014a) used ground- and ship-based observations to

16   estimate regional N_2O emissions and their interannual variability. Their study yielded global

17   fluxes for 1999-2009 that ranged from 17.5 to 20.1 Tg N yr^{-1}, with interannual variability

18   driven largely by fluctuations in tropical and subtropical soil fluxes. A recent intercomparison

19   of top-down inversion results using different transport models gave a comparable range of

20   global fluxes: 16.1-18.7 Tg N yr^{-1} for 2006-2009 (Thompson et al., 2014c).

21   Some previous work has found that uncertainties in stratosphere-troposphere exchange (STE)

22   and the associated influx of N_2O-depleted air can give rise to significant uncertainties in N_2O

23   source inversions, depending on the time range and scale ~~on~~ over which the emissions are

24   optimized (Nevison et al., 2005; Hirsch et al., 2006; Huang et al., 2008). On the other hand,

25   Thompson et al. (2011) found their a posteriori surface fluxes to be quite insensitive to biases

26   in the N_2O stratospheric loss rate during the first year of a multi-year simulation. They also

27   found that combining surface and aircraft observations could provide some constraint on the

28   magnitude of the stratospheric N_2O sink in a simultaneous source-sink inversion, without

29   increasing errors in the a posteriori N_2O emissions. However, biases in the model STE itself

30   did give rise to regional uncertainties of up to 25% in the optimized source.

The global observing network for atmospheric N_2O includes flask-based measurements and quasi-continuous in-situ instruments, as well as both surface- and airborne sampling platforms. However, a full quantification of the relative utility of these different datasets has not yet been performed. Such information is needed in order to determine: *i)* the degree to which current observations can be used to constrain N_2O emissions and stratospheric loss, and the comparative value of different observing strategies for doing so; *ii)* the spatial and temporal resolution at which N_2O sources and sinks can be constrained by these different datasets; and *iii*) where additional measurements are most needed to advance present understanding of the atmospheric N_2O budget.

In this paper, we introduce a new simulation and inversion framework for atmospheric N_2O using the GEOS-Chem chemical transport model (CTM) and its adjoint. The adjoint-based variational method is advantageous as it allows us to solve for N_2O fluxes at the spatial resolution of the CTM and at any desired time step, thus minimizing any impact from aggregation errors. Here, we apply the model in a simulation environment (i.e., in observing system simulation experiments, or OSSEs) to quantify the N_2O source and sink constraints provided by: *i*) flask and quasi-continuous surface observations from a number of long-term monitoring networks; *ii*) routine flask observations from an instrument platform deployed onaboard a commercial aircraft (Civil Aircraft for the Regular Investigation of the atmosphere Based on an Instrument Container; CARIBIC); and *iii*) in situ airborne observations made during a series of intensive pole-to-pole field campaigns (HIAPER Pole-to-Pole Observations; HIPPO). This is the first study to quantify the individual constraints provided by these different observation ensembles. We determine the potential for model errors in the stratospheric loss rate of N_2O to bias the inferred emission estimates, and assess how well N_2O emissions and stratospheric loss can be simultaneously constrained by the above observations. We evaluate the temporal and spatial resolution of emission constraints afforded by the different N_2O observations, and explore the impact of uncertainties in the a priori error estimates on the inferred fluxes. Finally, we apply the above information to identify regions that are underconstrained by the current N_2O observing network, and the downwind locations where new measurements would be most valuable for reducing current uncertainty in the N_2O budget.

2   N$_2$O simulation in the GEOS-Chem CTM

In this work we implement an N$_2$O simulation in the GEOS-Chem (http://www.geos-chem.org) global 3-D model of atmospheric chemistry. Analyses presented here use GEOS 5 assimilated meteorological data from the NASA Goddard Earth Observing System (GEOS-5), degraded to a horizontal resolution of 4° latitude × 5° longitude and to a vertical grid containing 47 levels from the surface to 0.01 hPa. Transport is calculated on a 30 minute time step; a 60 minute time step is used for emissions and chemistry. Our simulation period runs from April 2010 to April 2012.

A priori N$_2$O emissions are grouped into four categories: anthropogenic sources (including industrial processes, transportation, residential/waste management, and agricultural activities), natural soil fluxes, biomass burning, and oceanic exchange. Annual emissions for anthropogenic activities are obtained from the Emission Database for Global Atmospheric Research (EDGARv4.2, http://edgar.jrc.ec.europa.eu). Within this database there are 12 emission sectors as defined by the IPCC (IPCC, 2006). These sectors are listed in Table 1, along with the corresponding total emissions for 2008. The overall anthropogenic N$_2$O flux from EDGARv4.2 is 6.9 Tg N yr^{-1}, with 2.4 Tg N yr^{-1} from industrial and residential sources and 4.5 Tg N yr^{-1} from direct and indirect agricultural emissions. Natural soil emissions of N$_2$O are computed based on the EDGARv2 database, which provides an annual flux at 1° × 1° resolution for the year 1990 totaling 3.2 Tg N yr^{-1}. Biomass burning emissions of N$_2$O are prescribed monthly based on the Global Fire Emissions Database version 3 (GFEDv3, van der Werf et al., 2010) and total 0.6 Tg N yr^{-1} for 2010-2011. Thermal and biogeochemical oceanic fluxes of N$_2$O are calculated monthly at 4.5° × 3.75° following Jin and Gruber (2003), leading to a net annual global source of 3.5 Tg N yr^{-1}. Figure 1 maps the resulting annual flux from soils, anthropogenic activities, biomass burning, and air-sea exchange, with a cumulative annual global source of 14.2 Tg N yr^{-1}. We note that this is below the range of current top-down flux estimates (~16 to 20 Tg N yr^{-1}) discussed previously.

Stratospheric destruction of N$_2$O by photolysis and reaction with O(^{1}D) is calculated using archived monthly 3-D loss frequencies from Global Modeling Initiative (GMI) simulations driven by Modern Era Retrospective-Analysis for Research and Applications (MERRA) meteorological fields (MERRA is also based on GEOS-5). The resulting stratospheric loss gives rise to a 127.5 year lifetime, which is in the range of current estimates (122-131 years,

14

Formatted: Superscript

1   Volk et al., 1997; Prather et al., 2012). This lifetime depends upon the initial mass distribution

2   assumed for N_2O, which we describe below.

3   Because of the long atmospheric lifetime of N_2O, generating realistic initial conditions is of

4   critical importance for top-down analyses of its sources and sinks. Some previous studies have

5   included initial conditions as part of the state vector for optimization, or prescribed N_2O mass

6   fields from simulations that have reached a pseudo-steady state. We instead construct an

7   initial 3-D N_2O field using global observations for March 2010 (Fig. 2), one month prior to

8   the start of our optimization window. This timing is chosen to accommodate a brief model

9   spin-up that smooths any artificial horizontal gradients prescribed in the initial conditions.

10   Initial tropospheric concentrations are computed from NOAA Carbon Cycle and Greenhouse

11   Gases (CCGG) flask observations (described below) averaged monthly and zonally at 4°

12   resolution. These mixing ratios are then assumed uniform from the surface to the tropopause.

13   Above 100 hPa, our initial conditions are based on monthly mean (March 2010) N_2O profiles

14   measured by the Microwave Limb Sounder (MLS) onboard the EOS Aura satellite (Lambert

15   et al., 2007) interpolated onto the GEOS-Chem horizontal and vertical grid. Where needed,

16   we then perform a linear interpolation between the tropopause and 100 hPa.

17

18   **3   Inversion set-up and verification**

19   We use a 4D-Var inversion framework to solve for spatially resolved, monthly N_2O fluxes

20   based on the atmospheric measurements described next (Section 4). Optimal fluxes are

21   derived by minimizing the cost function, $J(\boldsymbol{p})$, which contains contributions from the error

22   weighted model-measurement differences and a penalty term:

23   $$J(\boldsymbol{p}) = \frac{1}{2}\sum_{c\in\Omega}(\boldsymbol{c}-\boldsymbol{y})^T \mathbf{S}_y^{-1}(\boldsymbol{c}-\boldsymbol{y}) + \frac{1}{2}\gamma(\boldsymbol{p}-\boldsymbol{p}_a)^T \mathbf{S}_a^{-1}(\boldsymbol{p}-\boldsymbol{p}_a) \qquad (1)$$

24   Here, $\boldsymbol{p}$ is the vector of parameters to be optimized, $\boldsymbol{p}_a$ is the initial (a priori) value of those

25   parameters, $\boldsymbol{y}$ is a set of observations, $\boldsymbol{c}$ is a vector containing the model-simulated

26   concentrations, $\mathbf{S}_y$ and $\mathbf{S}_a$ are the observational and a priori emissions error covariance

27   matrices, respectively, $\boldsymbol{\Omega}$ is the time and space domain of the observations, and γ is a

28   regularization parameter (set here to 1.0).

15

In this study, $\boldsymbol{p}$ contains monthly scaling factors for the terrestrial and oceanic emissions of N_2O and for stratospheric loss frequencies. The adjoint model calculates the gradient of the cost function with respect to this state vector, $\nabla_p J(\boldsymbol{p})$, and employs a quasi-Newton minimization routine to iteratively minimize $J(\boldsymbol{p})$ (Zhu et al., 1994; Byrd et al., 1995). Scale factors for emissions are optimized on the $4° \times 5°$ GEOS-Chem grid, while those for the stratospheric loss frequencies are aggregated over the vertical extent of the stratosphere and into eight latitude bands of $22.5°$. For the two-year inversion, tThis results in a state vector with 79,488 elements for emissions and 192 elements for stratospheric loss. We use a lower bound of zero in the optimization routine to avoid a solution containing negative scaling factors and an upper bound of 10 that was found to improve optimization performance. Use of the lower bound corresponds to an implicit assumption that the sign of the a priori N_2O flux in each location is correct (i.e. ocean regions with net N_2O uptake will remain net sinks) are no stronger of a sink than in the prior, while the upper bound corresponds to an assumptionassumes that the a priori emissions are not biased low by more than a factor of 10. These Such assumptions bounds are not problematic for the synthetic experiments presented here, but could be when performingwould affect real inversions if those assumptions were violated .

We assume 100% uncertainty in the a priori emissions (for any given grid square and month) and in the stratospheric loss frequencies, and impose horizontal correlation length scales for emissions of 500 km over land and 1000 km over ocean, following Thompson et al. (2011; 2014a). The observational error covariance matrix contains contributions from the measurement uncertainty (typically 0.4 ppb, see next section for details) and from model transport errors. We estimate the latter from the variance in modeled N_2O mixing ratios across all grid boxes adjacent to that containing a given observation. At the surface, tThis results in a mean errors of 0.2 ppb at the surface and; however, it results in a mean error of 2-8 ppb at aircraft cruising altitudes.

The adjoint modules for optimizing N_2O emissions and stratospheric loss were verified by comparing adjoint and finite difference sensitivities calculated for each atmospheric column with no horizontal transport. We find good agreement between adjoint and finite difference sensitivities for both emissions and stratospheric loss scaling factors (Fig. S1), demonstrating the accuracy of the N_2O adjoint code. Propagation of adjoint sensitivities through horizontal

16

transport in the GEOS-Chem adjoint has been verified previously (Henze et al., 2007). The GEOS-Chem adjoint has been used for a wide range of research applications such as constraining sources of aerosols (Henze et al., 2007; Henze et al., 2009; Kopacz et al., 2011; Wang et al., 2012; Xu et al., 2013), CO (Kopacz et al., 2009; Kopacz et al., 2010), NH_3 (Zhu et al., 2013), O_3 (Zhang et al., 2009; Parrington et al., 2012), and methanol (Wells et al., 2014), and to assess the impact of different types of observations on CO source inversions (Jiang et al., 2011; Jiang et al., 2013).

4   Global observations of atmospheric N_2O

Below, we apply GEOS-Chem and its adjoint to assess the N_2O source and sink constraints provided by the current suite of global observations. We include in this assessment several long-term surface monitoring networks and two aircraft platforms. A full list of the surface observation sites can be found in Table 2, and their locations are mapped in Fig. 3. The majority of the surface observations are from discrete air samples collected approximately weekly in flasks at 77 sites in the NOAA CCGG program (Dlugokencky et al., 1994), which are analyzed using a gas chromatograph with an electron capture detector and reported on the NOAA 2006A calibration scale. We also use flask measurements from six sites in the Commonwealth Scientific and Industrial Research Organisation (CSIRO) network (also on the NOAA 2006A scale; Francey et al, 1996; Cooper et al., 1999), five sites in the Environment Canada (EC) network (NOAA 2006 scale), and one National Institute of Water and Atmospheric research (NIWA) site (NOAA 2006A scale). We assume a measurement uncertainty of 0.4 ppb for all of the above flask measurements, based on recommendations from the data providers. Hourly averages of quasi-continuous measurements are employed from six sites in the NOAA Chromatograph for Atmospheric Trace Species (CATS) network, six sites in the Advanced Global Atmospheric Gases Experiment (AGAGE) network (Prinn et al., 2000), and the University of Minnesota tall tower Trace Gas Observatory (KCMP tall tower) site (Griffis et al., 2013). Measurements from the AGAGE network are reported on the SIO-98 scale, and have a reported uncertainty of 0.2% (0.6 ppb). Measurements at the KCMP tall tower and those in the CATS network (both on the NOAA 2006A scale) have uncertainties of about 1.0 and 0.3 ppb, respectively.

Extensive airborne measurements of N_2O are available from the ~~Civil Aircraft for the Regular Investigation of the atmosphere Based on an Instrument Container~~ (CARIBIC~~)~~ observatory (Brenninkmeijer et al., 2007). CARIBIC provides flask measurements from a commercial Lufthansa aircraft, with data available for 79 flights between Frankfurt, Germany and a number of other cities around the world (Fig. 3) during the time period of our optimization. These observations have an uncertainty of about 0.35 ppb and are reported on the NOAA 2006 scale (Schuck et al., 2009). Since the CARIBIC observatory is operated on a passenger aircraft, the majority of measurements are taken at a cruising altitude of 9-12 km: about 50% <u>are in the lowermost stratosphere</u> (in general those at higher latitudes, depending on synoptic conditions)~~ are in the lowermost stratosphere~~, with the remainder sampling the upper troposphere (Assonov et al., 2013; Umezawa et al., 2014).

High-frequency airborne N_2O measurements were made by quantum cascade laser spectroscopy (QCLS) during the ~~HIAPER Pole to Pole Observations~~ (HIPPO~~)~~ campaigns (Wofsy, 2011; flight tracks mapped in Fig. 3). Three of the five HIPPO deployments took place during our optimization window: HIPPO III (24 March – 16 April 2010), HIPPO IV (14 June – 11 July 2011), and HIPPO V (9 August – 9 September 2011), totaling 33 flights over the April 2010 – April 2012 time frame. Measurements are reported on the NOAA 2006 scale (Kort et al., 2011). The HIPPO flights range from pole-to-pole while profiling the atmosphere from the surface to the tropopause at regular intervals. Unlike the other available datasets, which provide recurrent measurements at discrete locations or along specific flight paths, the HIPPO datasets provide ~1-month global cross-sections of atmospheric concentration.

The use of different calibration scales results in offsets between different networks measuring N_2O, which may also vary with time. Because variability in atmospheric N_2O is low, these offsets can have a significant impact on the a posteriori solution. As the results presented here involve synthetic observations at the time and location of the real observations, we do not consider the impact of these offsets on inferred N_2O emissions and stratospheric loss. However, for inversions employing real N_2O measurements, we calculate offsets at collocated sites to adjust those measurements that are not reported on the NOAA 2006A scale.

5 Evaluating constraints on N$_2$O emissions and stratospheric loss using pseudo observations

In this section we perform a range of pseudo observation tests to determine how well N$_2$O sources (and sinks) can be quantified, and at what space-time resolution, based on the observing network described above. In these tests, we sample the model at the time and location of each observation to generate pseudo observations. A subset of ~~Most~~ tests were carried out with~~do not include~~ observational (measurement + transport) noise added to the synthetic observations, and these ~~m, but a subset of tests including noise~~ yielded the same results as the tests with no noise. We then perform a two-year inversion in which we assimilate pseudo observations generated for the surface network, CARIBIC flights, or HIPPO flights~~, or for a combination of those datasets~~. Our state vector contains monthly scaling factors for emissions, stratospheric loss frequencies, or both. We start with a spatially-uniform incorrect a priori value for these scaling factors; this bias is temporally -uniform in most tests, though later we also test the impact of a seasonally- varying emission bias ~~on the emissions~~. T~~t~~he degree to which the optimization converges to the true value of 1.0 for each grid cell and month gives a measure of the ability of the observations to correct for model biases in these processes. Section 5.1 presents ~~the~~ tests in which we optimize emissions using the three observational datasets, Section 5.2 contains ~~the~~ tests in which we optimize stratospheric loss frequencies alone or jointly with emissions, and Section 5.3 describes tests in which we optimize emissions with a seasonal a priori bias imposed. A full list of all pseudo observation tests performed is given in Table 3.

5.1 Constraints on N$_2$O emissions

Figure 4 shows the results of synthetic inversions in which we optimize emissions using~~based on~~ surface-based pseudo observations as described above. Here we impose a time invariant a priori emission bias of $\pm 50\%$ across all land and ocean grid cells, while keeping the stratospheric loss rates fixed at their true model values. We see that for the first ~20 months of the optimization window, the surface-based inversion is able to correct the imposed bias over most land and ocean regions that have a significant flux. However we will show later that this does not mean current observations can fully constrain the spatial distribution of N$_2$O emissions at the $4° \times 5°$ resolution shown in Fig. 4.

19

1 Overall, the solution is of comparable quality whether we start with a high or low a priori bias,

2 with some minor distinctions: the test with the positive initial bias performs slightly better

3 over oceans and in later months of the simulation, and also converges more quickly (5

4 iterations versus 10 for the test with a low initial bias). However, the situation is very different

5 when no upper bound is imposed on the solution. In this case, when given a low initial bias

6 the optimization tends to overshoot the truth in high-flux regions while underestimating the

7 truth in low-flux regions. Imposing both lower and upper bounds on the inverse solution (in

8 this case, 0 and 10) is thus important to ensure a consistent solution across high and low initial

9 bias scenarios. Jiang et al. (2014) concluded that construction of the a priori constraint was the

10 most important factor affecting the consistency of solutions for divergent initial assumptions

11 in the case of CO; we find here that the prior bounds placed on the solution can have a

12 comparable impact for N_2O.

13 Figure 4 also indicates that during the last several months of the optimization window there is

14 inadequate forcing for the inversion to completely correct for the initial emission biases,

15 particularly over the Southern Hemisphere. This is largely due to the timescale required to

16 transport N_2O between source regions and receptor locations—in the Southern Hemisphere

17 observing stations are sparse and distant from major N_2O sources. As a result, there are

18 relatively few subsequent observations that are influenced by biases imposed towards the end

19 of the optimization window.

20 Figure 5 shows zonally integrated, annual a posteriori emissions from synthetic inversions

21 using surface, CARIBIC, or HIPPO pseudo observations. In each case the state vector for

22 optimization includes monthly emission scale factors on the model grid (but not stratospheric

23 loss rates), and an initial bias of ±50% is applied to emissions in all grid boxes. Results are

24 shown only for the first year of the optimization period since (as shown) the inversion has less

25 ability to retrieve the true emissions in the succeeding months; there are also no HIPPO

26 observations during the last six months of the simulation. As discussed, the surface data

27 provide a good correction to the imposed a priori error in N_2O emissions when starting with

28 both high and low initial biases, and can accurately retrieve zonally integrated emissions in

29 the Northern and Southern Hemispheres.

30 We see in Fig. 5 that inversions based on the HIPPO data are also able to capture the zonal

31 distribution of N_2O emissions. For the high-bias test (a priori emissions scaling factor of 1.5),

20

the inversion results are very similar to those obtained using the surface data. For the low-bias test, the a posteriori emissions retain a low bias over the Southern Ocean, and overshoot slightly where emissions peak in both hemispheres. On the other hand, the CARIBIC measurements lead to substantially different a posteriori fluxes between the high- and low-bias tests: the inversion with the high initial bias returns the true zonal distribution of emissions quite well, whereas the test with the low initial bias leads to an overestimate of emissions from 20° - 30° N and an underestimate elsewhere. We find through these tests that each dataset can independently resolve the global annual flux to within 5% of the true value (Table 3).

Based on these experiments, we conclude that relatively sparse observations in the upper troposphere and lowermost stratosphere such as those from CARIBIC are sufficient to correct a prior bias in the global annual N_2O emissions, but do not provide as robust a constraint on the zonal distribution of those emissions. The pole-to-pole HIPPO observations, ~~which~~with their extensive vertical ~~contain~~ profil~~es~~ing from the upper troposphere to the boundary layer, provide a stronger constraint on the zonal distribution of annual emissions despite the fact that they do not cover the full time period of our optimization. This is because the long lifetime of N_2O allows emissions perturbations to impact concentrations far from source regions 2-6 months after the perturbation (Thompson et al., 2014a). Of the three networks examined here (surface, CARIBIC, and HIPPO) in isolation, the regular surface measurements provide the best correction of annual emission biases.

The above OSSEs were performed based on an initial fractional emission bias that is uniform in space and time (i.e., a priori emissions set everywhere to 0.5× or 1.5× the true model values). As we will see later, emission biases that vary in space or time are much more difficult to resolve, due to the sparse observing network combined with the long atmospheric lifetime of N_2O.

5.2 Stratospheric loss of N_2O: Constraints from the observing network and impact on source inversions

An important finding from previous work is that N_2O emission estimates derived from surface concentration measurements can be biased by model errors in the stratospheric sink of N_2O (Thompson et al., 2011). Here, we explore the potential for the airborne observations provided

21

1   by CARIBIC and HIPPO, in conjunction with the surface network, to simultaneously

2   constrain N_2O ~~sinks as well as sources~~sources as well as sinks. To this end, we perform a

3   series of synthetic inversions with a prior bias imposed on the stratospheric loss frequencies

4   for N_2O (aggregated to eight equal latitude bands), and assess the degree to which we can

5   correct for errors in the N_2O sink (given a fixed N_2O source) or both the source and sink of

6   N_2O (simultaneously). As previously, a prior~~i~~ scaling factor~~s~~ of either 0.5 or 1.5 are~~is~~ applied

7   ~~to~~in each location and month, and we attempt to retrieve the true value of 1.0 in each case.

8   Figure 6 shows the resulting a posteriori scaling factors for stratospheric loss frequencies

9   when N_2O emissions are held fixed (and equal to their 'true' values). We can see that each

10   observational dataset provides some information to correct for biases in the loss frequencies in

11   the first year of the simulation. Stratospheric loss of N_2O in the second (i.e. final) year of the

12   inversion does not significantly affect ~~the~~ N_2O mixing ratios at the observation locations ~~of~~

13   ~~the observations~~, given ~~as~~that~~a~~ the ~~characteristic~~ timescale for ~~stratosphere to troposphere~~

14   mixing from the upper stratosphere (~~,~~where most of the N_2O loss occurs)~~,~~ to the troposphere

15   is~~of~~ 1-2 years (Salstein, 1995).~~;~~ Aa~~s~~ a result, the corresponding a posteriori scale factors do

16   not diverge significantly from their a prior~~i~~ values.

17   For the inversion using surface data, the optimized annual global sink in the first year of the

18   simulation is very close to the true value (Table 3), but the loss frequencies are only adjusted

19   throughout the first year in the tropics. In the extratropics, they adjust primarily during the

20   summer months. The extratropical timing corresponds to the observed seasonal minimum of

21   N_2O at these latitudes (Nevison et al., 2011). At their peaks, retrieved values in the Southern

22   Hemisphere approach the truth, whereas in the Northern Hemisphere they slightly overshoot

23   the true sink. A posteriori values near the poles remain close to the a priori in both

24   hemispheres. Solutions achieved using HIPPO or CARIBIC data are spatially similar to those

25   obtained with the surface observations, although the optimized global sink for both is biased

26   low (by 13-17%, Table 3) due to weaker forcing (fewer total observations, higher observation

27   uncertainty). Therefore, while all the observations provide some correction of biases in the

28   global stratospheric sink of N_2O given known surface fluxes (with the surface data providing

29   the strongest constraint), they provide limited information on the spatial and temporal

30   distribution of that sink.

Also shown in Fig. 6 are the a posteriori scaling factors for stratospheric loss frequencies of N_2O when both the source and sink are optimized simultaneously, and given an initial 50% low bias for each. In these tests, the sink does not return to the true value (Table 3); for the inversions using CARIBIC and HIPPO it actually moves slightly in the opposite direction (i.e. further from the truth than the a priori) due to the forcing imposed by the source bias. In other words, the inversion is not able to resolve a bias in N_2O emissions from a bias in the sink. Despite this behavior, the spatial distribution of the derived scaling factors for N_2O emissions (not shown) closely matches that obtained with a fixed ('true') stratospheric sink, and the annual a posteriori emission flux is within 5% of the truth (Table 3) for all tests except the high-bias test using CARIBIC pseudo-data. Therefore, on the 1-2 year timescale of our optimization, and given accurate initial conditions (in our case, based on interpolated measurements), the forcing provided by the surface and aircraft data used here is dominated by N_2O emissions. As a result, a model bias of up to 50% in the stratospheric loss frequencies for N_2O will have minimal impact on the inferred emissions given the inversion framework employed here.

Thompson et al. (2011) also examined the feasibility of constraining stratospheric loss rates of N_2O using aircraft observations, but assumed zero model transport error in the observational error covariance matrix. We find that proper treatment of this error has a dramatic effect on the ability of the inversion framework to simultaneously retrieve emissions and stratospheric loss rates of N_2O. In the tests above, the model transport error was estimated based on the variance in N_2O mixing ratios in the grid boxes adjacent to an observation; for aircraft observations near the tropopause, this variability can be an order of magnitude larger than it is near the surface. We find that when we omit the model transport error, the inversion is able to reduce an imposed prior bias in both emissions and stratospheric loss simultaneously, even when those biases have opposing effects on the N_2O burden. As observed above, the same is not true when transport error is accounted for. Our ability to quantify both the emissions and chemistry of N_2O based on aircraft data therefore depends critically on the accuracy of vertical transport in the model, and on the associated transport error assigned in the inversion. Tracer measurements and correlations from platforms such as The CARIBIC data may provecan be useful infor evaluating model transport in the upper troposphere/lower stratosphere; Sawa et al. (2015) recently found a seasonal signal in the gradient of N_2O

1. ~~between flight level and the tropopause which reflected the seasonal variability in transport~~
2. ~~between the stratosphere and troposphere~~this.

3. Along with the rate of N_2O destruction in the stratosphere, another factor that can affect N_2O
4. source inversions is model uncertainty in the mass flux of air between the stratosphere and
5. troposphere (e.g., Thompson et al., 2014b). Our model framework, employing assimilated
6. meteorology, is not equipped to include this process directly as part of the state vector for
7. optimization. However, we can explore the relative influence of chemistry versus
8. stratosphere-troposphere mixing on the tropospheric N_2O burden (and hence on N_2O source
9. inversions) with the aid of a simple two-box model representing stratospheric and
10. tropospheric reservoirs of N_2O. Such an analysis does not capture seasonal effects,
11. ~~transport~~distinct STE mechanisms ~~that occur~~operating on different timescales, or spatial
12. gradients within the troposphere and stratosphere, but nonetheless does illustrate some key
13. features of the system.

14. Figure 7 shows the fractional perturbations to the stratospheric and tropospheric burdens of
15. N_2O in the box model that result from: *i*) a 20% increase in the global N_2O emission source
16. (*E*); *ii*) a 20% decrease in the photochemical loss rate of N_2O (k_{chem}); and *iii*) a 20% decrease
17. in the stratosphere-troposphere exchange rates (k_{ST} and k_{TS}). For the latter, mass fluxes in both
18. directions are increased proportionately since the (annual, global) k_{ST}/k_{TS} ratio is known from
19. the relative sizes of the troposphere and stratosphere.

20. The top panel of Fig. 7 shows that on long timescales a perturbation to k_{ST} and k_{TS} has a
21. negligible effect on the tropospheric N_2O burden compared to a perturbation to k_{chem} or *E*. A
22. given change in k_{chem} or *E* leads to a similar relative change in the steady-state burden, with an
23. adjustment timescale dictated by the N_2O lifetime (~127 years). In comparison, the effect of a
24. change to k_{TS} and k_{ST} is small in the troposphere. For stratospheric N_2O, the effect of k_{TS} and
25. k_{ST} is somewhat larger and of opposite sign: decreasing k_{TS} and k_{ST} reduces stratospheric N_2O
26. while increasing tropospheric N_2O.

27. However, on short timescales (as is used for our inversions), the importance of stratosphere-
28. troposphere exchange versus chemistry for tropospheric N_2O is reversed, as the former
29. manifests more quickly. The bottom panel of Fig. 7 indicates that for the first 2 years
30. following a perturbation, the effect of k_{TS} and k_{ST} on the tropospheric N_2O burden is 1.3-29×
31. larger (mean: 5.1×) than the effect of k_{chem}. Over this same time period, Fig. 7 also shows that

24

1   the effect of a perturbation to k_{TS} and k_{ST} is significant (mean: 0.8×) relative to a change in E.

2   However, the importance of k_{TS} and k_{ST} versus E will be overstated by the box model as it

3   does not resolve spatial gradients within the troposphere or the location of observations

4   relative to emissions.

5   Overall, we can see that N_2O source inversions based on the framework employed here will

6   be unaffected by even relatively large model biases in the chemical loss rate of N_2O. The

7   same does not apply to model biases in STE, and these need to be accounted for when

8   evaluating a posteriori source estimates for N_2O (Thompson et al., 2014b) and other long-

9   lived species such as CO_2 (Deng et al, 2015).

10 ### 5.3   Temporal resolution of N_2O source inversions

11 The OSSEs in Sections 5.1 and 5.2 demonstrate that the inversion (and N_2O observing

12 network) has a strong ability to remove model emission biases that are uniform in space and

13 time. However, actual model emission errors are likely to be spatially and temporally

14 dependent. For example, while the a priori natural soil and anthropogenic emissions used here

15 are aseasonal, observations over an agricultural field in Ontario, Canada indicate that 30-90%

16 of the annual flux occurs in the non-growing season, mostly as strong pulses driven by soil

17 thawing (Wagner-Riddle et al., 2007). Likewise, analysis of tall tower observations suggest a

18 strong seasonal cycle of soil N_2O emissions associated with the timing of fertilizer application

19 (Miller et al., 2012; Griffis et al., 2013). A key question, therefore, is the following: At what

20 spatial and temporal resolution can global N_2O emissions be quantified based on the current

21 observing network?

22 To explore the temporal aspect of this question, we performed a test in which we assimilate

23 pseudo observations generated with aseasonal (model truth) emissions while imposing a

24 simple seasonal bias in the a priori emissions from natural and agricultural soils (50% higher

25 than model truth from March – August; 50% lower from September – February). As before,

26 we assimilate surface, CARIBIC, or HIPPO observations, and retrieve monthly scaling factors

27 for terrestrial and oceanic N_2O emissions.

28 Results of this test indicate that a seasonal, global, emission bias is much more difficult to

29 resolve than is a constant bias based on the current network of surface observations. Zonally-

25

integrated emissions (Fig. S2) begin to approach the aseasonal model truth in the Northern Hemisphere during the beginning of the simulation (when the a priori emissions are biased high), but there is almost no correction of the seasonal bias in the latter half of the simulation (when a priori emissions are biased low). Due to the long lifetime of N_2O, any residual high emission bias from the first portion of the simulation leads to positive model-measurement residuals even after the emission bias changes sign. Globally, the result is an annual flux that is biased slightly low (~5%; Table 3) and with incorrect seasonality.

In areas near measurement sites, however, some seasonal constraints are afforded in the inversion. For example, Fig. 8 shows monthly fluxes at four locations: a site with continuous observations (KCMP Tall Tower), a site with flask observations (Hegyhátsál, Hungary), a location in eastern China that is upwind of surface flask observations, and a remote site in the Democratic Republic of Congo (DR Congo). At the beginning of the simulation there is a substantial correction of the emission bias at the in situ (KCMP), flask (Hungary), and upwind (East China) sites. During the latter half of the year, when the a priori emissions are biased low, those errors are reduced as a result of the inversion at all three sites, but for the sites with measurements there is a time lag and subsequent overcorrection afterward. There is no significant correction to the biased DR Congo emissions during any point of the year.

Based on the above test, we can conclude that flask and in situ observations provide valuable corrections to seasonal emission biases upwind and in the vicinity of the measurements, though not necessarily on a monthly timescale. However, any seasonal biases arising from errors in model STE may be difficult to separate from such seasonal emission errors. Furthermore, large parts of the world (illustrated by the DR Congo site in Fig. 8) lack any meaningful seasonal constraints on emissions.

5.4 Spatial resolution of N_2O source inversions

The spatial resolution at which current measurements constrain global N_2O emissions in this inversion framework can be inferred from the reduction in emission errors that results from the ~~inversion~~assimilation. Here, we calculate this relative error reduction from a stochastic estimate of the inverse Hessian of the cost function (Eq. 1). For a reasonably linear model, the inverse Hessian approximates the a posteriori error covariance matrix of the emissions, and can be written:

1 $(\nabla^2 J(\boldsymbol{x}))^{-1} = (\mathbf{S}_a^{-1} + \mathbf{H}^T \mathbf{S}_y^{-1} \mathbf{H})^{-1} \approx \mathbf{S}_{post}$ (2)

2 where $\mathbf{H}$ is the tangent linear of the forward model, $\mathbf{S}_{post}$ is the a posteriori error covariance

3 matrix, and $\mathbf{S}_a$ and $\mathbf{S}_y$ are the a priori and observational error covariance matrices,

4 respectively, as in Eq. 1. Following Bousserez et al. (2015), we estimate $\nabla^2 J(\boldsymbol{x})$ using an

5 ensemble (500 members here) of stochastic cost function gradients, each generated by adding

6 Gaussian random noise to the pseudo observations according to the reported uncertainty of

7 each dataset. The reduction in $\mathbf{S}_{post}(i,j)$ relative to $\mathbf{S}_a(i,j)$ for any model grid cell (i,j) then

8 represents the ability of our observing system to remove a random emission error in that

9 location, in the absence of any large-scale source bias.

10 Figure 9 shows the resulting percent error reduction achieved in each model grid cell using

11 surface, CARIBIC, or HIPPO observations for a given month of our two-year simulation.

12 Results using surface observations are shown for month 1 (April 2010), but are comparable

13 for all subsequent months. We see appreciable error reduction near sites with continuous

14 observations in North America and Europe, and more modest error reductions in surrounding

15 grid cells, at sites with flask observations, and in the northern Atlantic upwind of Europe.

16 There is little ($< 5\%$) error reduction achieved throughout the tropics, Southern Hemisphere,

17 and high latitudes, except near Cape Grim, Australia where continuous observations are

18 available. The spatial distribution of the error reduction results is similar to the spatial

19 distribution of scaling factor adjustments in a pseudo observation inversion in which a

20 spatially-random bias has been applied (not shown).

21 Figure 9 also shows that the sparse, high altitude CARIBIC observations provide limited

22 information on the spatial distribution of N_2O emissions. Significant error reduction is

23 achieved over Western Europe during April 2010, the only month in which measurements

24 were taken in the lower troposphere during special flights dedicated to volcano observation

25 (Rauthe-Schöch, 2012). In all other months, measurements occur primarily in the upper

26 troposphere and lower stratosphere and consequently the spatial error reduction is minor

27 (typically $< 1\ \%$).

28 The spatial information provided by HIPPO observations varies by month according to the

29 flight tracks, and is complementary to that achieved with surface data. For example, during

30 August 2011, we see large error reductions over the central US, as well as some improvement

27

for grid cells in East Asia that are upwind of the HIPPO flight track. Some error reduction is also achieved in these locations for May 2011, despite the fact that no HIPPO flights occurred during this month (the next flights occurred in June). Given the long lifetime of N_2O, measurements in a given month thus provide some location-specific constraints on emissions in prior months. As is the case with the surface observations, however, the HIPPO data provides very little error reduction for emissions throughout the tropics, Southern Hemisphere and high latitudes. While the OSSE tests above showed that our observation and adjoint framework has significant skill in removing uniform model emission biases, we see in Fig. 9 that our current ability to allocate those N_2O emissions spatially around the globe is in fact severely limited relative to the $4° \times 5°$ model resolution used here – and this is true for the airborne as well as the ground-based datasets.

Based on the same stochastic approach used above to calculate the inverse Hessian, we can also calculate the averaging kernel of the inversion. ~~Because t~~The averaging kernel ~~is a~~ measure~~s~~ ~~of~~ the sensitivity of the inversion ~~results in a particular location~~ to emissions in ~~each~~any given grid square; ~~,~~ we can thus use it to determine how well emissions in a given location can be independently resolved from emissions ~~in other locations~~elsewhere. If emissions in one location are completely resolved from those in other grid boxes, the averaging kernel value will be 1.0 in that location and 0 everywhere else. Here, we calculate the averaging kernel rows (based on the surface observations only) for a selected group of locations in key emission regions that vary in their proximity to N_2O measurement sites.

Figure 10 shows the results for four locations: the KCMP Tall Tower (MN, USA; 44.68° N, 93.07 W), Hegyhátsál (Hungary; 46.95° N, 16.65° E), East China (30.0° N, 115.0° E), and the Democratic Republic of Congo (2.0° N, 30.0° E). KCMP features continuous observations, and we see that emissions in this model grid cell can be constrained independently (averaging kernel value near 1.0, and near 0.0 elsewhere) from those in other places. Significant constraints are achieved at Hegyhátsál (averaging kernel value ~0.3), where weekly flask observations are available, though some spatial smearing is apparent. Weaker constraints (averaging kernel values up to ~0.03) are achieved in the vicinity of the East China grid box, likely provided by downwind observations in Korea and the western Pacific.

Averaging kernel values for the Central Africa location are very low (~10^{-3}), indicating little to no constraint on the source flux, and are also highly smeared spatially, showing that the

28

current surface observations of N_2O do not allow emissions in that region to be independently resolved from emissions elsewhere across the globe. We see in Fig. 10 that this spatial smearing even extends to the midlatitudes in both hemispheres. Emissions in the underconstrained tropics thus risk being conflated with those in other, distant source regions in global inversion analyses.

The implications of this current lack of constraints on tropical N_2O emissions can be seen in a sample global inversion based on real atmospheric data. Figure 11 shows a posteriori emission scaling factors for global inversions based on two different assumptions: the first uses our previous construction of the a priori error covariance matrix (100% uncertainty with horizontal correlation length scales of 500 km over land and 1000 km over ocean); the other does not include any penalty term (measuring the departure from a priori conditions) in the cost function. When a priori constraints are included, the solution is relatively spatially smooth. To correct for a low bias in our a priori emissions inventory, emissions increase throughout those terrestrial and oceanic regions where emissions occur, with a slightly higher inferred flux over South America. Conversely, when we eliminate the a priori constraint, emissions increase strongly in the tropics and Southern Hemisphere, reaching a factor of 10 (the upper bound placed on the scaling factors) in South America near the beginning of the two-year simulation. To compensate for this, the inferred emissions throughout the Northern Hemisphere decrease dramatically.

This severe sensitivity of the solution to the a priori error assumption reflects the ill-posed nature of the problem. It also highlights the fact that, because the global N_2O flux is constrained (as the N_2O lifetime and atmospheric burden are reasonably well-known), the lack of constraint on tropical emissions has important implications for understanding emissions elsewhere in the world.

5.5   Identifying priority locations for future N_2O measurements

In this section, we apply the error reduction statistics derived above to identify priority regions where new observations are likely to have high value for improving present understanding of global N_2O sources. To that end, we carry out forward model simulations in which N_2O emissions in the first month are scaled by $(1 - x)$, where x is the spatial map of relative error reductions achieved in the inversion on the basis of the surface observations (e.g., Fig. 9). The

29

1 initial atmospheric burden of N_2O is set to zero, as are the emissions in subsequent months.

2 The resulting atmospheric N_2O then reflects unconstrained emissions, and the distribution of

3 that 'unconstrained N_2O' in space and time shows where new observations are needed to

4 quantify those emissions in a spatially explicit way.

5 Figure 12 shows the distribution of unconstrained N_2O mapped in the first and the second

6 month following its emission. Results are shown for simulations starting in August 2010 and

7 February 2011; these months were chosen to illustrate how seasonal differences in horizontal

8 and vertical transport affect the atmospheric dispersion of underconstrained N_2O emissions. In

9 August, unconstrained mixing ratios above 1 ppb can be found throughout Southeast Asia,

10 Central Africa, and South America, with the highest concentrations occurring over Brazil and

11 off the western coasts of Africa and South America. Somewhat elevated concentrations (0.5-1

12 ppb) persist in these locations for the second month of the simulation, but these become well-

13 dispersed in the following months (not shown). Unconstrained N_2O emitted in August is

14 initially concentrated in the lower troposphere in the tropics and northern midlatitudes, but is

15 lofted through the tropical troposphere by September. In contrast, unconstrained N_2O emitted

16 in February is more strongly confined to the lower troposphere and the Northern Hemisphere,

17 even a month after emission.

18 The maps in Fig. 12 rely by necessity on a particular a priori estimate of N_2O emissions and

19 their distribution in space and time. However, they nonetheless provide an assessment of

20 where additional measurements would have the best leverage for improving N_2O emission

21 estimates, based on our existing bottom-up understanding of when and where those emissions

22 occur. We see in the maps that areas over or downwind of the tropics and East Asia should

23 receive the highest measurement priority to reduce uncertainty in the overall N_2O budget. As

24 shown earlier, downwind surface observations can provide some spatially explicit emission

25 constraints for regions with high fluxes; these may be the only feasible option for places

26 where access, infrastructure, or political issues prevent sustained local measurements. We

27 note that additional N_2O measurements are now available in and around Japan (Saikawa et al.,

28 2013) that may provide additional constraints on East Asian emissions not achieved using the

29 measurements presented here. In addition, aircraft measurements during the July-September

30 timeframe should have strong value for constraining fluxes in the tropics, given the lofting

31 and dispersal of those emissions that is apparent in the August 2010 simulation. The value of

30

Ssuch measurements was also pointed out by Kort et al. (2011), who reported ~~may be particularly useful for N2O given the~~ observational evidence for lofting of large, episodic tropical emissions ~~in the tropics (Kort et al., 2011)~~. On the other hand, Fig. 12 also reveals large areas of the world's oceans where additional surface measurements are not likely to provide appreciable new insights into the global N_2O budget, given the lack of unconstrained N_2O that is less than 1-2 months from emission.

6   Summary and conclusions

We developed a new inversion framework based on the GEOS-Chem model and its adjoint for estimating global N_2O emissions and stratospheric loss rates using surface (~~combined~~ flask~~;~~ and in-situ) as well as airborne (CARIBIC; HIPPO) measurements. We used this framework to: *i*) quantify the ability of the current observing network to constrain the global distribution of N_2O sources and sinks; *ii*) assess the relative utility of the various observing platforms for doing so; and *iii*) identify priority locations where measurements are most needed to improve present understanding of the N_2O budget. Our simulation period runs from April 2010 to April 2012, with initial conditions constructed using surface flask observations and vertical profile measurements from the MLS satellite sensor.

Observing system simulation experiments (OSSEs) showed that the surface and HIPPO observations can accurately resolve a uniform bias in N_2O emissions for the first year of a two-year simulation; in comparison, the sparser (and mostly high altitude) CARIBIC observations provide a weaker constraint. All three datasets are able to independently resolve the global surface flux to within 5% of the truth. On the other hand, a seasonal emission bias is much more difficult to resolve given the long lifetime of N_2O, particularly in regions with sparse observations. The surface observations do provide a reduction of seasonal emission errors in the vicinity of measurement sites and in large source regions upwind.

The surface and airborne datasets are all able to resolve a global bias in the stratospheric loss rate of N_2O given known emissions, but do not give information on the spatial and temporal distribution of that sink. For the more realistic scenario with uncertain N_2O sources and sink, we find that resolving the two in a joint source-sink inversion would require greater confidence in modeled transport than is currently warranted. Nevertheless, because of the

31

1 timescale for stratosphere-troposphere mixing, N_2O source inversions are insensitive to
2 uncertainties in the chemical sink of N_2O on the 2 year analysis time frame used here (and
3 assuming an accurate initial state; e.g. from interpolated data). However, a simple box model
4 analysis shows that tropospheric N_2O is more sensitive to uncertainties in the rate of
5 stratosphere-troposphere exchange (STE) than to those in the chemical loss rates for analysis
6 timescales up to ~3-4 years. Incomplete knowledge of STE rates will thus be a key source of
7 uncertainty to address for N_2O source inversions on these timescales.

8 We employed a stochastic estimate of the inverse Hessian to quantify the spatial resolution of
9 N_2O emission constraints afforded by the current global network of observations, and the
10 degree to which emissions in a particular location can be distinguished from those elsewhere.
11 Significant location-specific constraints are achieved in grid boxes near and immediately
12 upwind of surface observation locations; however, these are mainly confined to North
13 America, Europe and Australia. For sites with continuous surface observations, local
14 emissions can be unambiguously resolved from those in surrounding locations, as indicated
15 by large error reductions and averaging kernel (AK) values close to 1.0. Flask observations
16 also provide significant local-to-regional constraints (e.g., AK values of ~0.3 at a site with
17 weekly measurements). HIPPO observations primarily provide emission constraints for the
18 Central US and East Asia. Critically, little to no spatial information on tropical emissions is
19 provided by either set of observations: the corresponding AKs are highly smeared spatially
20 and show that emissions in many parts of the tropics cannot even be resolved from those in
21 the midlatitudes. For global inversions, this underconstraint in the tropics can thus lead to
22 large errors in the inferred N_2O fluxes for the extratropics as well as the tropics themselves.

23 From the atmospheric distribution of 'unconstrained N_2O' simulated based on the error
24 reduction statistics achieved in the inversion and our a priori source estimates, we identify
25 areas in the tropics and East Asia as the highest priorities for new N_2O measurements to
26 advance understanding of the global budget. In situ or flask observations downwind of major
27 sources in South America, Central Africa, and East Asia can provide some spatial information
28 on N_2O fluxes in cases where local, long-term measurements are impractical. Targeted aircraft
29 measurements in the troposphere could also provide much-needed constraints on tropical
30 emission fluxes, particularly during July-September when emissions are well-lofted vertically.

From our analysis it is clear that additional measurements are crucial to obtaining a more complete picture of global N_2O sources, particularly in the key areas mentioned above. In this context, we will further investigate the use of efficient randomization techniques to estimate the spatiotemporal constraints provided by new and existing N_2O measurements, and design optimal dimension approaches for N_2O source inversions. Such work could also include an evaluation of information provided by new N_2O retrievals from AIRS (Xiong et al., 2014) and other space-based infrared sounders. While the vertical sensitivity of such instruments may be insufficient to derive useful direct information on surface emissions, such data could be useful for constraining the N_2O profile and its stratosphere-troposphere exchange (thus indirectly improving our ability to diagnose sources). The fact that the current observing system yields little information on the space-time distribution of N_2O fluxes over large parts of the world also speaks to the need for process-based emission models that can provide a priori source estimates that faithfully capture the key modes of variability. Such models are also needed to project how soil N_2O fluxes will respond to future changes in climate, hydrology, and nitrogen deposition and runoff.

Acknowledgments

Code availability

The N$_2$O version of the GEOS-Chem adjoint code is available via the GEOS-Chem adjoint repository. Instructions for obtaining access to the code can be found at wiki.seas.harvard.edu/geos-chem/index.php/GEOS-Chem_Adjoint.

References

Assonov, S. S., Brenninkmeijer, C. A. M., Schuck, T., and Umezawa, T.: N$_2$O as a tracer of mixing stratospheric and tropospheric air based on CARIBIC data with applications for CO$_2$, Atmos. Environ., 79, 769-779, doi:10.1016/j.atmosenv.2013.07.035, 2013.

Bousserez, N., Henze, D. K., Perkins, A., Bowman, K. W., Lee, M., Liu, J., Deng, F., and Jones, D. B. A., Improved analysis-error covariance matrix for high-dimensional variational inversions: application to source estimation using a 3D atmospheric transport model, Q. J. Roy. Meteor. Soc., doi:10.1002/qj.2495, 2015.

Bouwman, A. F.: Environmental science - Nitrogen oxides and tropical agriculture, Nature, 392, 866-867, doi:10.1038/31809, 1998.

Bouwman, A. F., Beusen, A. H. W., Griffioen, J., Van Groenigen, J. W., Hefting, M. M., Oenema, O., Van Puijenbroek, P. J. T. M., Seitzinger, S., Slomp, C. P., and Stehfest, E.: Global trends and uncertainties in terrestrial denitrification and N$_2$O emissions, Philos. T. Roy Soc. B, 368, 20130112, doi:10.1098/rstb.2013.0112, 2013.

Brenninkmeijer, C. A. M., Crutzen, P., Boumard, F., Dauer, T., Dix, B., Ebinghaus, R., Filippi, D., Fischer, H., Franke, H., Friess, U., Heintzenberg, J., Helleis, F., Hermann, M., Kock, H. H., Koeppel, C., Lelieveld, J., Leuenberger, M., Martinsson, B. G., Miemczyk, S., Moret, H. P., Nguyen, H. N., Nyfeler, P., Oram, D., O'Sullivan, D., Penkett, S., Platt, U., Pupek, M., Ramonet, M., Randa, B., Reichelt, M., Rhee, T. S., Rohwer, J., Rosenfeld, K., Scharffe, D., Schlager, H., Schumann, U., Slemr, F., Sprung, D., Stock, P., Thaler, R., Valentino, F., van Velthoven, P., Waibel, A., Wandel, A., Waschitschek, K., Wiedensohler, A., Xueref-Remy, I., Zahn, A., Zech, U., and Ziereis, H.: Civil Aircraft for the regular investigation of the atmosphere based on an instrumented container: The new CARIBIC system, Atmos. Chem. Phys., 7, 4953-4976, doi:10.5194/acp-7-4953-2007, 2007.

1   Butterbach-Bahl, K., Baggs, E. M., Dannenmann, M., Kiese, R., and Zechmeister-Boltenstern,

2   S.: Nitrous oxide emissions from soils: how well do we understand the processes and their

3   controls?, Philos. T. Roy Soc. B, 368, 20140122, doi:10.1098/rstb.2013.0122, 2013.

4   Byrd, R. H., Lu, P. H., Nocedal, J., and Zhu, C. Y.: A limited memory algorithm for bound

5   constrained optimization, SIAM J. Sci. Comput., 16, 1190-1208, doi:10.1137/0916069, 1995.

6   Cohen, Y., and Gordon, L. I.: Nitrous oxide production in the ocean, J. Geophys. Res.-Oc.

7   Atm., 84, 347-353, doi:10.1029/JC084iC01p00347, 1979.

8   Cooper, L. N., Steele, L. P., Langenfelds, R. L., Spencer, D. A., and Lucarelli, M. P.:

9   Atmospheric methane, carbon dioxide, hydrogen, carbon monoxide and nitrous oxide from

10 Cape Grim flask air samples analysed by gas chromatography, Baseline Atmospheric Program

11 (Australia) 1996, 98 - 102, Bureau of Meteorology and CSIRO Atmospheric Research, 1999.

12 Davidson, E. A.: The contribution of manure and fertilizer nitrogen to atmospheric nitrous

13 oxide since 1860, Nat. Geosci., 2, 659-662, doi:10.1038/ngeo608, 2009.

14 Deng, F., Jones, D. B. A., Walker, T. W., Keller, M., Bowman, K. W., Henze, D. K., Nassar,

15 R., Kort, E. A., Wofsy, S. C., Walker, K. A., Bourassa, A. E., and Degenstein, D. A.:

16 Sensitivity analysis of the potential impact of discrepancies in stratosphere-troposphere

17 exchange on inferred sources and sinks of CO_2, Atmos. Chem. Phys. Discuss., 15, 10813-

18 10851, doi:10.5194/acpd-15-10813-2015, 2015.

19 Denman, K. L., Brasseur, G. P., Chidthaisong, A., Ciais, P., Cox, P. M., Dickinson, R. E.,

20 Hauglustaine, D., Heinze, C., Holland, E., Jacob, D., Lohmann, U., Ramachandran, S., da

21 Silva Dias, P. L., Wofsy, S. C., and Zhang, X.: Couplings Between Changes in the Climate

22 System and Biogeochemistry, in: Climate Change 2007: Contribution of Working Group I to

23 the Fourth Assessment Report of the Intergovernmental Panel on Climate Change, edited by:

24 Solomon, S. D., Qin, D., Manning, M., Chen, Z., Marquis, M., Averyt, K. B., Tignor, M., and

25 Miller, H. L., Cambridge University Press, Cambridge, 499-587, 2007.

26 Dlugokencky, E. J., Steele, L. P., Lang, P. M., and Masarie, K. A.: The growth rate and

27 distrubution of atmospheric methane, J. Geophys. Res.-Atmos., 99, 17021-17043,

28 doi:10.1029/94JD01245, 1994.

Firestone, M. K., and Davidson, E. A.: Microbiological basis of NO and N_2O production and consumption in the soil, in: Exchange of Trace Gases Between Terrestrial Ecosystems and the Atmosphere, edited by: Andreae, M. O., and Schimel, D. S., Wiley and Sons, Chichester, 7-21, 1989.

Forster, P., Ramaswamy, V., Artaxo, P., Berntsen, T., Betts, R., Fahey, D. W., Haywood, J., Lean, J., Lowe, D. C., Myrhe, G., Nganga, J., Prinn, R., Raga, G., Schulz, M., and Van Doorland, R.: Changes in atmospheric constituents and in radiative forcing, Cambridge, United Kingdom, and New York, NY, USA, 2007.

Elkins, J. W., Wofsy, S. C., McElroy, M. B., Kolb, C. E., and Kaplan, W. A.: Aquatic sources and sinks for nitrous oxide, Nature, 275, 602-606, 1978.

Francey, R. J., Steele, L. P., Langenfelds, R. L., Lucarelli, M. P., Allison, C. E., Beardsmore, D. J., Coram, S. A., Derek, N., de Silva, F. R., Etheridge, D. M., Fraser, P. J., Henry, R. J., Turner, B., Welch, E. D., Spencer, D. A., and Cooper, L. N.,: Global Atmospheric Sampling Laboratory (GASLAB): supporting and extending the Cape Grim trace gas programs, Baseline Atmospheric Program (Australia) 1993, 8-29, Bureau of Meteorology and CSIRO division of Atmospheric Research, 1996.

Galloway, J. N., Townsend, A. R., Erisman, J. W., Bekunda, M., Cai, Z. C., Freney, J. R., Martinelli, L. A., Seitzinger, S. P., and Sutton, M. A.: Transformation of the nitrogen cycle: Recent trends, questions, and potential solutions, Science, 320, 889-892, doi:10.1126/science.1136674, 2008.

Griffis, T. J., Lee, X., Baker, J. M., Russelle, M. P., Zhang, X., Venterea, R., and Millet, D. B.: Reconciling the differences between top-down and bottom-up estimates of nitrous oxide emissions for the US Corn Belt, Global Biogeochem. Cy., 27, 746-754, doi:10.1002/gbc.20066, 2013.

Henze, D. K., Hakami, A., and Seinfeld, J. H.: Development of the adjoint of GEOS-Chem, Atmos. Chem. Phys., 7, 2413-2433, doi:10.5194/acp-7-4953-2007, 2007.

Henze, D. K., Seinfeld, J. H., and Shindell, D. T.: Inverse modeling and mapping US air quality influences of inorganic $PM_{2.5}$ precursor emissions using the adjoint of GEOS-Chem, Atmos. Chem. Phys., 9, 5877-5903, doi:10.5194/acp-9-5877-2009, 2009.

Hirsch, A. I., Michalak, A. M., Bruhwiler, L. M., Peters, W., Dlugokencky, E. J., and Tans, P. P.: Inverse modeling estimates of the global nitrous oxide surface flux from 1998-2001, Global Biogeochem. Cy., 20, GB1008, 17, doi:10.1029/2004gb002443, 2006.

Huang, J., Golombek, A., Prinn, R., Weiss, R., Fraser, P., Simmonds, P., Dlugokencky, E. J., Hall, B., Elkins, J., Steele, P., Langenfelds, R., Krummel, P., Dutton, G., and Porter, L., Estimation of regional emissions of nitrous oxide from 1997 to 2005 using multinetwork measurements, a chemical transport model, and an inverse method, J. Geophys. Res., 113, D17313, doi:10.1029/2007JD009381, 2008.

IPCC: 2006 IPCC Guidelines for National Greenhouse Gas Inventories, edited by: Eggleston, H. S., Buendia, L., Miwa, K., Ngara, T., and Tanabe, K., IGES, Japan, 2006.

Jiang, Z., Jones, D. B. A., Kopacz, M., Liu, J., Henze, D. K., and Heald, C.: Quantifying the impact of model errors on top-down estimates of carbon monoxide emissions using satellite observations, J. Geophys. Res.-Atmos, 116, D15306, doi:10.1029/2010JD015282, 2011.

Jiang, Z., Jones, D. B. A., Worden, H. M., Deeter, M. N., Henze, D. K., Worden, J., Bowman, K. W., Brenninkmeijer, C. A. M., and Schuck, T. J.: Impact of model errors in convective transport on CO source estimates inferred from MOPITT CO retrievals, J. Geophys. Res., 118, 2073-2083, doi:10.1002/jgrd.50216, 2013.

Jin, X., and Gruber, N.: Offsetting the radiative benefit of ocean iron fertilization by enhancing N_2O emissions, Geophys. Res. Lett., 30, 2249, doi:10.1029/2003GL018458, 2003.

Kopacz, M., Jacob, D. J., Henze, D. K., Heald, C. L., Streets, D. G., and Zhang, Q.: Comparison of adjoint and analytical Bayesian inversion methods for constraining Asian sources of carbon monoxide using satellite (MOPITT) measurements of CO columns, J. Geophys. Res.-Atmos., 114, D04305, doi:10.1029/2007JD009264, 2009.

Kopacz, M., Jacob, D. J., Fisher, J. A., Logan, J. A., Zhang, L., Megretskaia, I. A., Yantosca, R. M., Singh, K., Henze, D. K., Burrows, J. P., Buchwitz, M., Khlystova, I., McMillan, W. W., Gille, J. C., Edwards, D. P., Eldering, A., Thouret, V., and Nedelec, P.: Global estimates of CO sources with high resolution by adjoint inversion of multiple satellite datasets (MOPITT, AIRS, SCIAMACHY, TES), Atmos. Chem. Phys., 10, 855-876, doi:10.5194/acp-10-855-2010, 2010.

37

Kopacz, M., Mauzerall, D. L., Wang, J., Leibensperger, E. M., Henze, D. K., and Singh, K.: Origin and radiative forcing of black carbon transported to the Himalayas and Tibetan Plateau, Atmos. Chem. Phys., 11, 2837-2852, doi:10.5194/acp-11-2837-2011, 2011.

Kort, E. A., Patra, P. K., Ishijima, K., Daube, B. C., Jimenez, R., Elkins, J., Hurst, D., Moore, F. L., Sweeney, C., Wofsy, S. C.: Tropospheric distribution and variability of N_2O: Evidence for strong tropical emissions, Geophys. Res. Lett., 38, L15806, doi:10.1029/2011GL047612, 2011.

Lambert, A., Read, W. G., Livesey, N. J., Santee, M. L., Manney, G. L., Froidevaux, L., Wu, D. L., Schwartz, M. J., Pumphrey, H. C., Jimenez, C., Nedoluha, G. E., Cofield, R. E., Cuddy, D. T., Daffer, W. H., Drouin, B. J., Fuller, R. A., Jarnot, R. F., Knosp, B. W., Pickett, H. M., Perun, V. S., Snyder, W. V., Stek, P. C., Thurstans, R. P., Wagner, P. A., Waters, J. W., Jucks, K. W., Toon, G. C., Stachnik, R. A., Bernath, P. F., Boone, C. D., Walker, K. A., Urban, J., Murtagh, D., Elkins, J. W., and Atlas, E.: Validation of the Aura Microwave Limb Sounder middle atmosphere water vapor and nitrous oxide measurements, J. Geophys. Res.-Atmos., 112, D24S36, doi:10.1029/2007JD008724, 2007.

Law, C. S., and Owens, N. J. P.: Significant flux of atmospheric nitrous oxide from the northwest Indian Ocean, Nature, 346, 826-828, doi:10.1038/346826a0, 1990.

Maggiotto, S. R., Webb, J. A., Wagner-Riddle, C., and Thurtell, G. W.: Nitrous and nitrogen oxide emissions from turfgrass receiving different forms of nitrogen fertilizer, J. Environ. Qual., 29, 621-630, 2000.

Miller, S. M., Kort, E. A., Hirsch, A. I., Dlugokencky, E. J., Andrews, A. E., Xu, X., Tian, H., Nehrkorn, T., Eluszkiewicz, J., Michalak, A. M., and Wofsy, S. C.: Regional sources of nitrous oxide over the United States: Seasonal variation and spatial distribution, J. Geophys. Res.-Atmos., 117, D06310, doi:10.1029/2011JD016951, 2012.

Mosier, A., Kroeze, C., Nevison, C., Oenema, O., Seitzinger, S., and van Cleemput, O.: Closing the global N_2O budget: nitrous oxide emissions through the agricultural nitrogen cycle - OECD/IPCC/IEA phase II development of IPCC guidelines for national greenhouse gas inventory methodology, Nutr. Cycl. Agroecosys., 52, 225-248, doi:10.1023/a:1009740530221, 1998.

38

Nevison, C. D., Keeling, R. F., Weiss, R. F., Popp, B. N., Jin, X., Fraser, P. J., Porter, L. W., and Hess, P. G.: Southern Ocean ventilation inferred from seasonal cycles of atmospheric N_2O and O_2/N_2 at Cape Grim, Tasmania, Tellus B, 57, 218-229, doi:10.1111/j.1600-0889.2005.00143.x, 2005.

Nevison, C. D., Dlugokencky, E., Dutton, G., Elkins, J. W., Fraser, P., Hall, B., Krummel, P. B., Langenfelds, R. L., O'Doherty, S., Prinn, R. G., Steele, L. P., and Weiss, R. F.: Exploring causes of interannual variability in the seasonal cycles of tropospheric nitrous oxide, Atmos. Chem. Phys., 11, 3713-3730, doi:10.5194/acp-11-3713-2011, 2011.

Park, S., Croteau, P., Boering, K. A., Etheridge, D. M., Ferretti, D., Fraser, P. J., Kim, K. R., Krummel, P. B., Langenfelds, R. L., van Ommen, T. D., Steele, L. P., and Trudinger, C. M.: Trends and seasonal cycles in the isotopic composition of nitrous oxide since 1940, Nat. Geosci., 5, 261-265, doi:10.1038/ngeo1421, 2012.

Parrington, M., Palmer, P. I., Henze, D. K., Tarasick, D. W., Hyer, E. J., Owen, R. C., Helmig, D., Clerbaux, C., Bowman, K. W., Deeter, M. N., Barratt, E. M., Coheur, P. F., Hurtmans, D., Jiang, Z., George, M., and Worden, J. R.: The influence of boreal biomass burning emissions on the distribution of tropospheric ozone over North America and the North Atlantic during 2010, Atmos. Chem. Phys., 12, 2077-2098, doi:10.5194/acp-12-2077-2012, 2012.

Potter, C. S., Matson, P. A., Vitousek, P. M., and Davidson, E. A.: Process modeling of controls on nitrogen trace gas emissions from soils worldwide, J. Geophys. Res.-Atmos., 101, 1361-1377, doi:10.1029/95JD02028, 1996.

Prather, M. J., Holmes, C. D., and Hsu, J.: Reactive greenhouse gas scenarios: Systematic exploration of uncertainties and the role of atmospheric chemistry, Geophys. Res. Lett., 39, L09803, doi:10.1029/2012GL051440, 2012.

Prinn, R. G., Weiss, R. F., Fraser, P. J., Simmonds, P. G., Cunnold, D. M., Alyea, F. N., O'Doherty, S., Salameh, P., Miller, B. R., Huang, J., Wang, R. H. J., Hartley, D. E., Harth, C., Steele, L. P., Sturrock, G., Midgley, P. M., and McCulloch, A.: A history of chemically and radiatively important gases in air deduced from ALE/GAGE/AGAGE, J. Geophys. Res., 105, 17751-17792, doi:10.1029/2000JD900141, 2000.

1 Rauthe-Schöch, A., Weigelt, A., Hermann, M., Martinsson, B. G., Baker, A. K., Heue, K. P.,
2 Brenninkmeijer, C. A. M., Zahn, A., Scharffe, D., Eckhardt, S.: CARIBIC aircraft
3 measurements of Eyjafjallajökull volcanic clouds in April/May 2010, Atmos. Chem. Phys.,
4 12, 879-902, 10.5194/acp-12-879-2012, 2012.

5 Ravishankara, A. R., Daniel, J. S., and Portmann, R. W.: Nitrous Oxide (N_2O): The Dominant
6 Ozone-Depleting Substance Emitted in the 21st Century, Science, 326, 123-125,
7 doi:10.1126/science.1176985, 2009.

8 Saikawa, E., Prinn, R. G., Dlugokencky, E., Ishijima, K., Dutton, G. S., Hall, B. D.,
9 Langenfelds, R., Tohjima, Y., Machida, T., Manizza, M., Rigby, M., O'Doherty, S., Patra, P.
10 K., Harth, C. M., Weiss, R. F., Krummel, P. B., van der Schoot, M., Fraser, P. J., Steele, L. P.,
11 Aoki, S., Nakazawa, T., and Elkins, J. W.: Global and regional emissions estimates for N_2O,
12 Atmos. Chem. Phys., 14, 4617-4641, doi:10.5194/acp-14-4617-2014, 2014.

13 Salstein, D. A.: Mean properties of the atmosphere, in: Composition, Chemistry, and Climate
14 of the Atmosphere, edited by: Singh, H. B., Van Nostrand Reinhold, New York, 19-49, 1995.

15 Schuck, T. J., Brenninkmeijer, C. A. M., Slemr, F., Xueref-Remy, I., and Zahn, A.:
16 Greenhouse gas analysis of air samples collected onboard the CARIBIC passenger aircraft,
17 Atmos. Meas. Tech., 2, 449-464, doi:10.5194/amt-2-449-2009, 2009.

18 Shcherbak, I., Millar, N., and Robertson, G. P.: Global metaanalysis of the nonlinear response
19 of soil nitrous oxide (N_2O) emissions to fertilizer nitrogen, P. Natl. Acad. Sci. USA, 111,
20 9199-9204, doi:10.1073/pnas.1322434111, 2014.

21 Thompson, R. L., Bousquet, P., Chevallier, F., Rayner, P. J., and Ciais, P.: Impact of the
22 atmospheric sink and vertical mixing on nitrous oxide fluxes estimated using inversion
23 methods, J. Geophys. Res.-Atmos., 116, D17307, doi:10.1029/2011JD015815, 2011.

24 Thompson, R. L., Chevallier, F., Crotwell, A. M., Dutton, G., Langenfelds, R. L., Prinn, R.
25 G., Weiss, R. F., Tohjima, Y., Nakazawa, T., Krummel, P. B., Steele, L. P., Fraser, P.,
26 O'Doherty, S., Ishijima, K., and Aoki, S.: Nitrous oxide emissions 1999 to 2009 from a global
27 atmospheric inversion, Atmos. Chem. Phys., 14, 1801-1817, doi:10.5194/acp-14-1801-2014,
28 2014a.

1 Thompson, R. L., Patra, P. K., Ishijima, K., Saikawa, E., Corazza, M., Karstens, U., Wilson,
2 C., Bergamaschi, P., Dlugokencky, E., Sweeney, C., Prinn, R. G., Weiss, R. F., O'Doherty, S.,
3 Fraser, P. J., Steele, L. P., Krummel, P. B., Saunois, M., Chipperfield, M., and Bousquet, P.:
4 TransCom N_2O model inter-comparison - Part 1: Assessing the influence of transport and
5 surface fluxes on tropospheric N_2O variability, Atmos. Chem. Phys., 14, 4349-4368,
6 doi:10.5194/acp-14-4349-2014, 2014b.

7 Thompson, R. L., Ishijima, K., Saikawa, E., Corazza, M., Karstens, U., Patra, P. K.,
8 Bergamaschi, P., Chevallier, F., Dlugokencky, E., Prinn, R. G., Weiss, R. F., O'Doherty, S.,
9 Fraser, P. J., Steele, L. P., Krummel, P. B., Vermeulen, A., Tohjima, Y., Jordan, A., Haszpra,
10 L., Steinbacher, M., Van der Laan, S., Aalto, T., Meinhardt, F., Popa, M. E., Moncrieff, J.,
11 and Bousquet, P.: TransCom N_2O model inter-comparison - Part 2: Atmospheric inversion
12 estimates of N_2O emissions, Atmos. Chem. Phys., 14, 6177-6194, doi:10.5194/acp-14-6177-
13 2014, 2014c.

14 Umezawa, T., Baker, A. K., Oram, D., Sauvage, C., O'Sullivan, D., Rauthe-Schoch, A.,
15 Montzka, S. A., Zahn, A., Brenninkmeijer, C. A. M.: Methyl chloride in the upper troposphere
16 observed by CARIBIC passenger aircraft observatory: Large-scale distributions and Asian
17 summer monsoon outflow, J. Geophys. Res.-Atmos., 119, 5542-5558,
18 doi:10.1002/2013JD021396, 2014.

19 van der Werf, G. R., Randerson, J. T., Giglio, L., Collatz, G. J., Mu, M., Kasibhatla, P. S.,
20 Morton, D. C., DeFries, R. S., Jin, Y., and van Leeuwen, T. T.: Global fire emissions and the
21 contribution of deforestation, savanna, forest, agricultural, and peat fires (1997-2009), Atmos.
22 Chem. Phys., 10, 11707-11735, doi:10.5194/acp-10-11707-2010, 2010.

23 Volk, C. M., Elkins, J. W., Fahey, D. W., Dutton, G. S., Gilligan, J. M., Loewenstein, M.,
24 Podolske, J. R., Chan, K. R., and Gunson, M. R.: Evaluation of source gas lifetimes from
25 stratospheric observations, J. Geophys. Res.-Atmos., 102, 25543-25564,
26 doi:10.1029/97JD02215, 1997.

27 Wagner-Riddle, C., Furon, A., McLaughlin, N. L., Lee, I., Barbeau, J., Jayasundara, S.,
28 Parkin, G., Von Bertoldi, P., and Warland, J.: Intensive measurement of nitrous oxide
29 emissions from a corn-soybean-wheat rotation under two contrasting management systems

over 5 years, Glob. Change Biol., 13, 1722-1736, doi:10.1111/j.1365-2486.2007.01388.x, 2007.

Wang, J., Xu, X., Henze, D. K., Zeng, J., Ji, Q., Tsay, S.-C., and Huang, J.: Top-down estimate of dust emissions through integration of MODIS and MISR aerosol retrievals with the GEOS-Chem adjoint model, Geophys. Res. Lett., 39, L08802, doi:10.1029/2012GL051136, 2012.

Wells, K. C., Millet, D. B., Cady-Pereira, K. E., Shephard, M. W., Henze, D. K., Bousserez, N., Apel, E. C., de Gouw, J., Warneke, C., and Singh, H. B.: Quantifying global terrestrial methanol emissions using observations from the TES satellite sensor, Atmos. Chem. Phys., 14, 2555-2570, doi:10.5194/acp-14-2555-2014, 2014.

Wofsy, S. C.: HIAPER Pole-to-Pole Observations (HIPPO): fine-grained, global-scale measurements of climatically important atmospheric gases and aerosols, Philos. T. Roy. Soc. A, 369, 2073-2086, doi:10.1098/rsta.2010.0313, 2011.

Xiong, X., Maddy, E. S., Barnet, C., Gambacorta, A., Patra, P. K., Sun, F., and Goldberg, M.: Retrieval of nitrous oxide from Atmospheric Infrared Sounder: Characterization and validation, J. Geophys. Res.-Atmos., 119, 9107-9122, doi:10.1002/2013JD021406, 2014.

Xu, X., Wang, J., Henze, D. K., Qu, W., and Kopacz, M.: Constraints on aerosol sources using GEOS-Chem adjoint and MODIS radiances, and evaluation with multisensor (OMI, MISR) data, J. Geophys. Res.-Atmos., 118, 6396-6413, doi:10.1002/jgrd.50515, 2013.

Zhang, L., Jacob, D. J., Kopacz, M., Henze, D. K., Singh, K., and Jaffe, D. A.: Intercontinental source attribution of ozone pollution at western US sites using an adjoint method, Geophys. Res. Lett., 36, L11810, doi:10.1029/2009GL037950, 2009.

Zhu, C., Byrd, R. H., Lu, P., and Nocedal, J.: L-BFGS-B: a limited memory FORTRAN code for solving bound constrained optimization problems, Tech. rep., Northwestern University, 1994.

Zhu, L., Henze, D. K., Cady-Pereira, K. E., Shephard, M. W., Luo, M., Pinder, R. W., Bash, J. O., and Jeong, G. R.: Constraining U.S. ammonia emissions using TES remote sensing observations and the GEOS-Chem adjoint model, J. Geophys. Res.-Atmos, 118, 3355-3368, doi:10.1002/jgrd.50166, 2013.

1

Table 1. N_2O emissions in the a priori database and their global annual totals.

Sector	IPCC code	Global annual source (Tg N yr^{-1})
Agricultural soil[a]	4C+4D	3.97
Indirect emissions from agriculture[a]	4D3	0.57
Energy manufacturing transformation[a]	1A1+1A2+1B1b	0.21
Non-road transportation[a]	1A3a+c+d+e	5.0E-2
Road transportation[a]	1A3b	0.14
Oil production and refineries[a]	1B2a	4.2E-3
Industrial process and product use[a]	2	0.85
Fossil fuel fires[a]	7A	4.8E-4
Manure management[a]	4B	0.21
Residential[a]	1A4	0.18
Waste solid and waste water[a]	6	0.24
Indirect N_2O from NO_x and NH_3[a]	7B+7C	0.45
Total anthropogenic[a]		**6.9**
Total natural soil[b]		**3.2**
Total biomass burning[c]		**0.6**
Total net ocean[d]		**3.5**

3 [a] From EDGARv4.2 for 2008

4 [b] From EDGARv2 for 1990

5 [c] From GFEDv3 (van der Werf et al., 2010)

6 [d] From Jin and Gruber (2003)

7

1   Table 2. Sites of surface flask and in situ N_2O observations used in this study

Location	Latitude	Longitude	Network[a]	Measurement type	Measurement scale
Arrival Heights, Antarctica	-77.80	166.67	NIWA	Flask	NOAA 2006A
Alert, Nunavut, Canada	82.45	-62.51	CCGG	Flask	NOAA 2006A
Argyle, Maine, USA	45.04	-68.68	CCGG	Flask	NOAA 2006A
Ascension Island	-7.97	-14.40	CCGG	Flask	NOAA 2006A
Assekrem, Algeria	23.26	5.63	CCGG	Flask	NOAA 2006A
Tereceira Island, Azores	38.77	-27.38	CCGG	Flask	NOAA 2006A
Baltic Sea, Poland	55.35	17.22	CCGG	Flask	NOAA 2006A
Boulder Atmospheric Observatory, Colorado, USA	40.05	-105.00	CCGG	Flask	NOAA 2006A
Baring Head, New Zealand	-41.41	174.87	CCGG	Flask	NOAA 2006A
Bukit Kototabang, Indonesia	-0.20	100.32	CCGG	Flask	NOAA 2006A
St. David's Head, Bermuda	32.37	-64.65	CCGG	Flask	NOAA 2006A
Tudor Hill, Bermuda	32.27	-64.88	CCGG	Flask	NOAA

					2006A
Barrow, Alaska, USA	71.32	-156.61	CCGG, CATS	Flask, in situ	NOAA 2006A
Black Sea, Constanta, Romania	44.18	28.67	CCGG	Flask	NOAA 2006A
Cold Bay, Alaska, USA	55.21	-162.72	CCGG	Flask	NOAA 2006A
Cape Ferguson, Australia	-19.28	147.05	CSIRO	Flask	NOAA 2006A
Cape Grim, Tasmania, Australia	-40.68	144.69	CCGG, AGAGE	Flask, in situ	NOAA 2006A, SIO-98
Churchill, Manitoba, Canada	58.75	-94.07	EC	Flask	NOAA 2006
Christmas Island	1.70	-157.15	CCGG	Flask	NOAA 2006A
Cape Rama, India	15.08	73.83	CSIRO	Flask	NOAA 2006A
Crozet Island	-46.43	51.85	CCGG	Flask	NOAA 2006A
Casey Station, Antarctica	-66.28	110.53	CSIRO	Flask	NOAA 2006A
Drake Passage	-59.00	-64.69	CCGG	Flask	NOAA 2006A
Easter Island	-27.16	-109.43	CCGG	Flask	NOAA 2006A
Estevan Point, British Columbia, Canada	49.38	-126.55	EC	Flask	NOAA 2006

East Trout Lake, Saskatchewan, Canada	54.33	-104.98	EC	Flask	NOAA 2006
Fraserdale, Ontario, Canada	49.88	-81.57	EC	Flask	NOAA 2006
Mariana Islands, Guam	13.39	144.66	CCGG	Flask	NOAA 2006A
Gunn Point, Australia	-12.25	131.05	CSIRO	Flask	NOAA 2006A
Halley Station, Antarctica	-75.61	-26.21	CCGG	Flask	NOAA 2006A
Hohenpeissenberg, Germany	47.80	11.02	CCGG	Flask	NOAA 2006A
Hegyhátsál, Hungary	46.95	16.65	CCGG	Flask	NOAA 2006A
Stórhofdi, Vestmannaeyjar, Iceland	63.40	-20.29	CCGG	Flask	NOAA 2006A
Izaña, Tenerife, Canary Islands	28.31	-16.50	CCGG	Flask	NOAA 2006A
Jungfraujoch, Switzerland	46.55	7.99	AGAGE	In situ	SIO-98
Key Biscayne, Florida, USA	25.67	-80.16	CCGG	Flask	NOAA 2006A
Cape Kumukahi, Hawaii, USA	19.52	-154.82	CCGG	Flask	NOAA 2006A
Park Falls, Wisconsin, USA	45.95	-90.27	CCGG	Flask	NOAA 2006A

Lac La Biche, Alberta, Canada	54.95	-112.45	CCGG	Flask	NOAA 2006A
Lulin, Taiwan	23.47	120.87	CCGG	Flask	NOAA 2006A
Lampedusa, Italy	35.52	12.62	CCGG	Flask	NOAA 2006A
Mawson Station, Antarctica	-67.62	62.87	CSIRO	Flask	NOAA 2006A
Mace Head, Ireland	53.33	-9.90	CCGG, AGAGE	Flask, in situ	NOAA 2006A, SIO-98
Sand Island, Midway Islands	28.21	-177.38	CCGG	Flask	NOAA 2006A
Mt. Kenya, Kenya	-0.06	37.30	CCGG	Flask	NOAA 2006A
Mauna Loa, Hawaii, USA	19.54	-155.58	CCGG, CATS	Flask, in situ	NOAA 2006A, NOAA 2006A
Macquarie Island, Australia	-54.48	158.97	CSIRO	Flask	NOAA 2006A
Gobabeb, Namibia	-23.58	15.03	CCGG	Flask	NOAA 2006A
Niwot Ridge, Colorado, USA	40.05	-105.55	CCGG, CATS	Flask, in situ	NOAA 2006A, NOAA 2006A
Ochsenkopf,	50.03	11.81	CCGG	Flask	NOAA

Germany					2006A
Pallas-Sammaltunturi, Finland	67.97	24.12	CCGG	Flask	NOAA 2006A
Pacific Ocean, Equator	0.00	-155.00	CCGG	Flask	NOAA 2006A
Pacific Ocean, 5 N	5.00	-151.00	CCGG	Flask	NOAA 2006A
Pacific Ocean, 10 N	10.00	-149.00	CCGG	Flask	NOAA 2006A
Pacific Ocean, 15 N	15.00	-145.00	CCGG	Flask	NOAA 2006A
Pacific Ocean, 20 N	20.00	-141.00	CCGG	Flask	NOAA 2006A
Pacific Ocean, 25 N	25.00	-139.00	CCGG	Flask	NOAA 2006A
Pacific Ocean, 30 N	30.00	-135.00	CCGG	Flask	NOAA 2006A
Pacific Ocean, 5 S	-5.00	-159.00	CCGG	Flask	NOAA 2006A
Pacific Ocean, 10 S	-10.00	-161.00	CCGG	Flask	NOAA 2006A
Pacific Ocean, 15 S	-15.00	-171.00	CCGG	Flask	NOAA 2006A
Pacific Ocean, 20 S	-20.00	-174.00	CCGG	Flask	NOAA 2006A
Pacific Ocean, 25 S	-25.00	-171.00	CCGG	Flask	NOAA 2006A

Pacific Ocean, 30 S	-30.00	-176.00	CCGG	Flask	NOAA 2006A
Pacific Ocean, 35 S	-35.00	180.00	CCGG	Flask	NOAA 2006A
Palmer Station, Antarctica	-64.92	-64.00	CCGG	Flask	NOAA 2006A
Point Arena, California, USA	38.96	-123.74	CCGG	Flask	NOAA 2006A
Ragged Point, Barbados	13.17	-59.43	CCGG, AGAGE	Flask, in situ	NOAA 2006A, SIO-98
Beech Island, South Carolina, USA	33.41	-81.83	CCGG	Flask	NOAA 2006A
Mahe Island, Seychelles	-4.68	55.53	CCGG	Flask	NOAA 2006A
Sable Island, Nova Scotia, Canada	43.93	-60.02	EC	Flask	NOAA 2006
Southern Great Plains, Oklahoma, USA	36.61	-97.49	CCGG	Flask	NOAA 2006A
Shemya Island, Alaska, USA	52.71	174.13	CCGG	Flask	NOAA 2006A
Tutuila, American Samoa	-14.25	-170.56	CCGG, CATS	Flask, in situ	NOAA 2006A, NOAA 2006A
South Pole, Antarctica	-89.98	-24.80	CCGG, CATS	Flask, in situ	NOAA 2006A,

					NOAA 2006A
Schauinsland, Germany	47.92	7.92	AGAGE	In situ	SIO-98
Sutro Tower, California, USA	37.76	-122.45	CCGG	Flask	NOAA 2006A
Summit, Greenland	72.60	-38.42	CCGG, CATS	Flask, in situ	NOAA 2006A, NOAA 2006A
Syowa Station, Antarctica	-69.01	39.59	CCGG	Flask	NOAA 2006A
Tae-ahn Peninsula, Korea	36.74	126.13	CCGG	Flask	NOAA 2006A
Tierra Del Fuego, Argentina	-54.85	-68.31	CCGG	Flask	NOAA 2006A
KCMP Tall Tower, Minnesota, USA	44.68	-93.07		In situ	NOAA 2006A
Trinidad Head, California, USA	41.05	-124.15	CCGG, AGAGE	Flask, in situ	NOAA 2006A, SIO-98
Wendover, Utah, USA	39.90	-113.72	CCGG	Flask	NOAA 2006A
Ulaan Uul, Mongolia	44.45	111.10	CCGG	Flask	NOAA 2006A
West Branch, Iowa, USA	41.73	-91.35	CCGG	Flask	NOAA 2006A
Walnut Grove,	38.27	-121.49	CCGG	Flask	NOAA

California, USA					2006A
WIS Station, Negev, Desert, Israel	30.86	34.78	CCGG	Flask	NOAA 2006A
Moody, Texas, USA	31.32	-97.33	CCGG	Flask	NOAA 2006A
Mt. Waliguan, China	36.29	100.90	CCGG	Flask	NOAA 2006A
Western Pacific Cruise	-30.00 to 30.00	136.80 to 168.00	CCGG	Flask	NOAA 2006A
Ny-Ålesund, Svalbard, Norway	78.91	11.89	CCGG	Flask	NOAA 2006A

1   [a] CCGG: NOAA Carbon Cycle and Greenhouse Gases program; EC: Environment Canada;

2   NIWA: National Institute of Water and Atmospheric research; CATS: NOAA Chromatograph

3   for Atmospheric Trace Species; AGAGE: Advanced Global Atmospheric Gases Experiment.

1   Table 3. Global annual N_2O a posteriori source for all pseudo observation tests

Observations	State vector	Initial bias	A posteriori flux (Tg N yr⁻¹)[a]	A posteriori sink (Tg N yr⁻¹)[b]
Surface	Emissions	0.5, 1.5	14.16, 14.25	--
CARIBIC	Emissions	0.5, 1.5	13.82, 14.72	--
HIPPO	Emissions	0.5, 1.5	14.12, 14.27	--
Surface	Emissions + Strat loss frequencies	0.5, 1.5	14.04, 14.84	7.73, 24.91
CARIBIC	Emissions + Strat loss frequencies	0.5, 1.5	13.63, 15.40	6.13, 19.72
HIPPO	Emissions + Strat loss frequencies	0.5, 1.5	14.00, 14.74	7.65, 22.60
Surface	Strat loss frequencies	0.5, 1.5		12.02, 12.93
CARIBIC	Strat loss frequencies	0.5, 1.5		10.09, 14.66
HIPPO	Strat loss frequencies	0.5, 1.5		10.60, 13.99
CARIBIC (no transport error)	Emissions + strat loss frequencies	0.5	14.16	9.94
HIPPO (no transport error)	Emissions + strat loss frequencies	0.5	14.14	11.39
CARIBIC (no transport error)	Strat loss frequencies	0.5		11.57
HIPPO (no transport error)	Strat loss frequencies	0.5		12.03
Surface	Emissions	Seasonal	13.63	

CARIBIC	Emissions	Seasonal	13.59
HIPPO	Emissions	Seasonal	13.44

1 [a] True model flux is 14.16 Tg N yr^{-1}

2 [b] True model stratospheric sink is 12.1 Tg N yr^{-1}

3

4
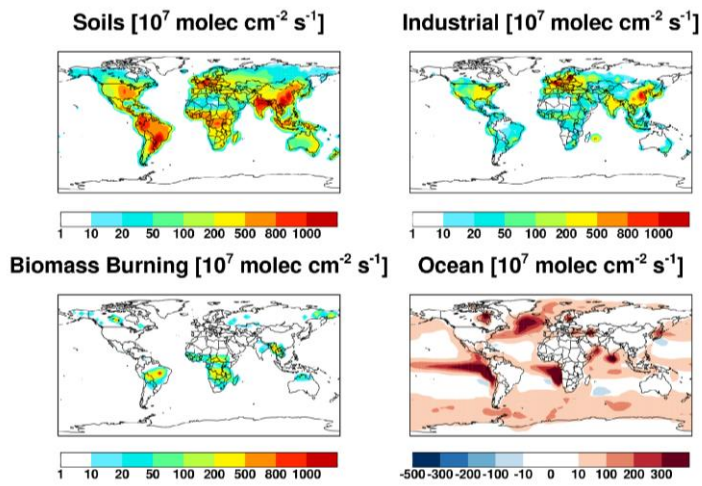
5

6 Figure 1. Mean annual N$_2$O fluxes from soils, industrial activities, biomass burning, and ocean

7 exchange in the GEOS-Chem a priori simulation.

8

9

201003 N₂O tropospheric mixing ratio

201003 N₂O zonal average mixing ratio
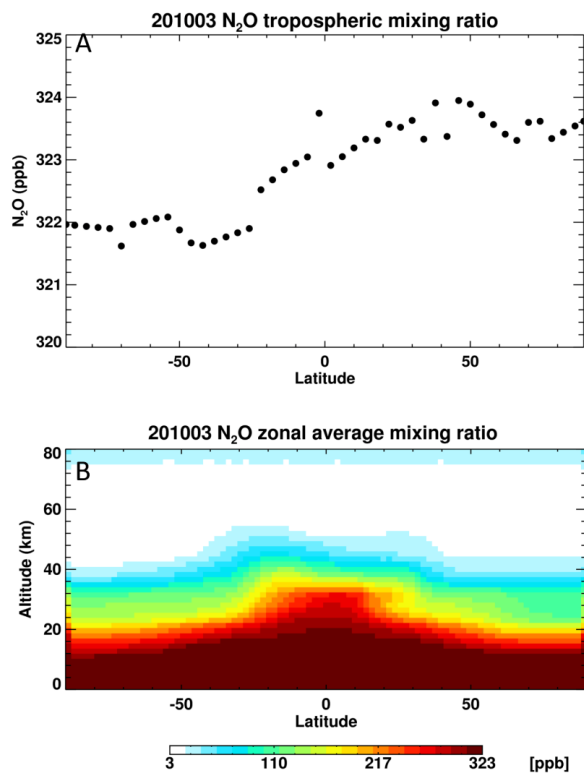
1

2   Figure 2. Initial model N_2O field for March 2010. Shown are the (A) tropospheric N_2O mixing

3   ratios, and (B) zonal mixing ratio cross-section.

4

5
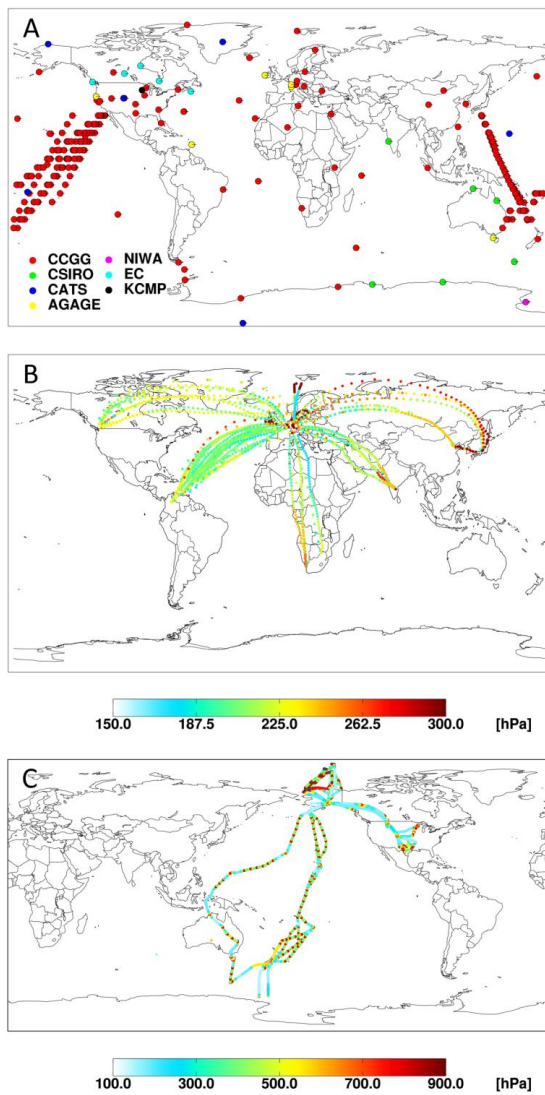
Figure 3. Global observing network for atmospheric N_2O. Shown are the locations of (A) surface observations, (B) CARIBIC aircraft observations, and (C) HIPPO aircraft observations. The CARIBIC and HIPPO flights are shaded by the pressure at which the observations were made. Color scales differ between panels (B) and (C) to show the range of vertical levels samplinged in each case.
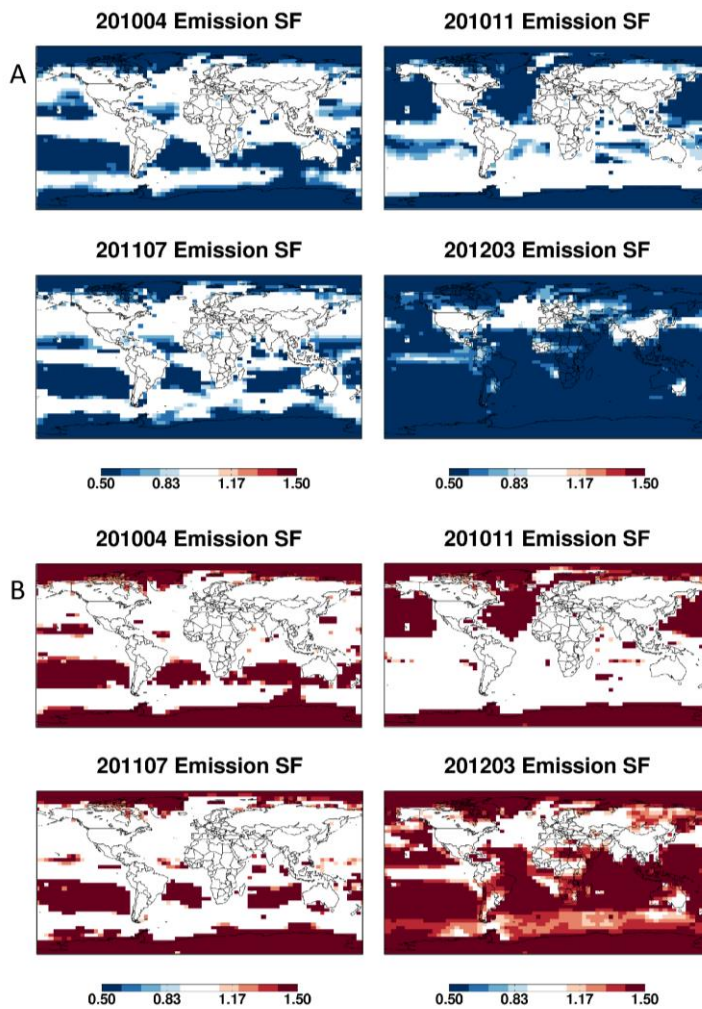
Figure 4. Pseudo observation test optimizing N_2O emissions on the basis of surface observations. Shown are a posteriori emission scaling factors using an a priori guess of either (A) 0.5 or (B) 1.5, where the true value is 1.0. Results are shown for April 2010 (month 1 of the inversion window), November 2010 (month 8), July 2011 (month 16), and March 2012 (month 24).
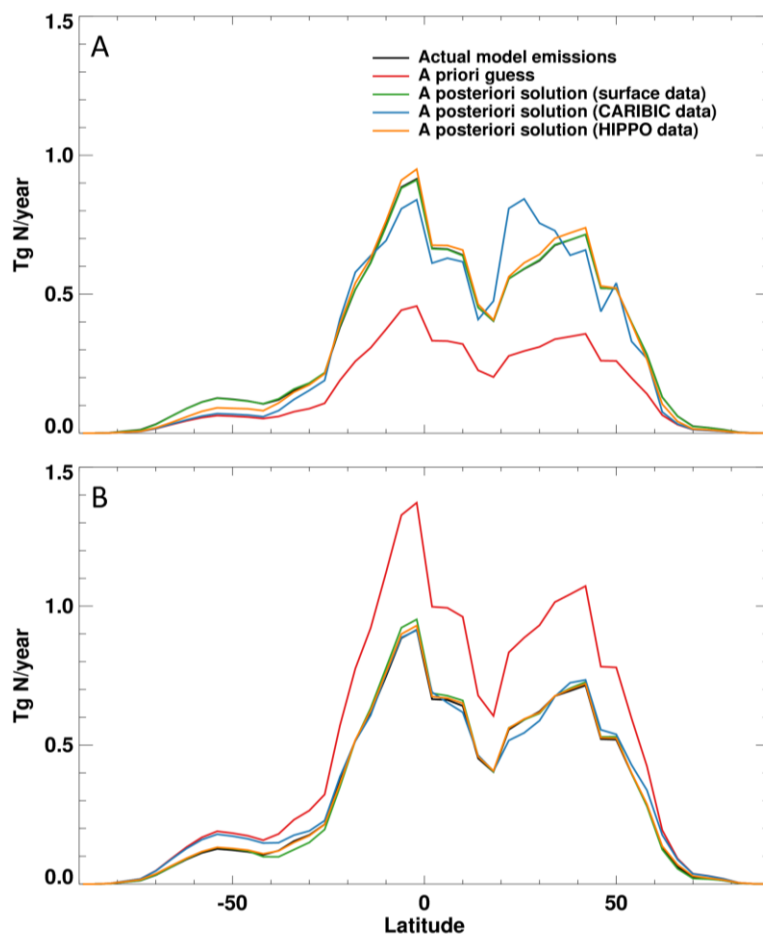
1

2 Figure 5. Pseudo observation tests optimizing N$_2$O emissions. Shown are zonally-integrated

3 annual emissions for the first year of the simulation (April 2010 – March 2011) starting with

4 an a priori scaling factor of (A) 0.5 and (B) 1.5, where the true value is 1.0. Actual model

5 emissions are shown in black, model emissions scaled by the a priori guess are shown in red,

6 and a posteriori emissions obtained using surface data, CARIBIC data, and HIPPO data are

7 shown in green, blue, and yellow, respectively.

1
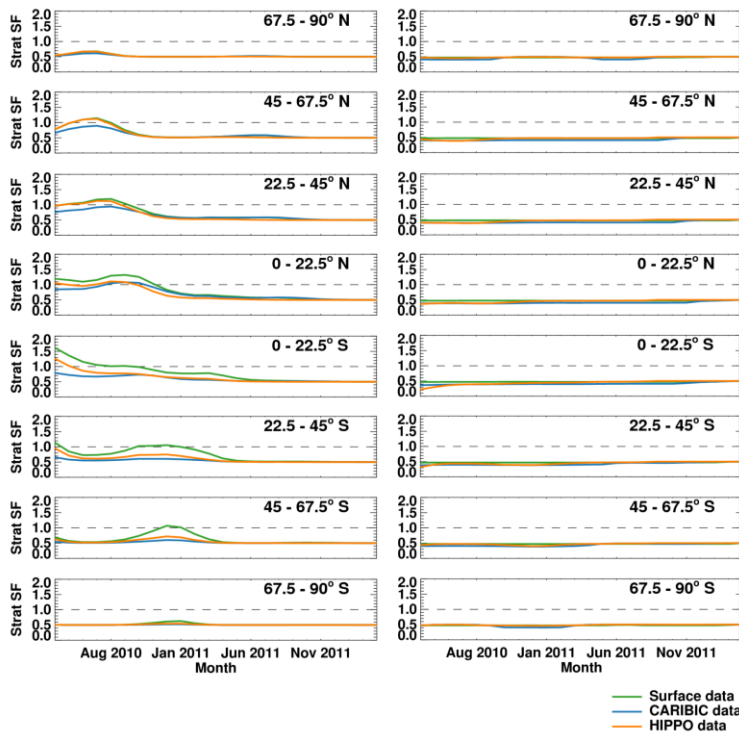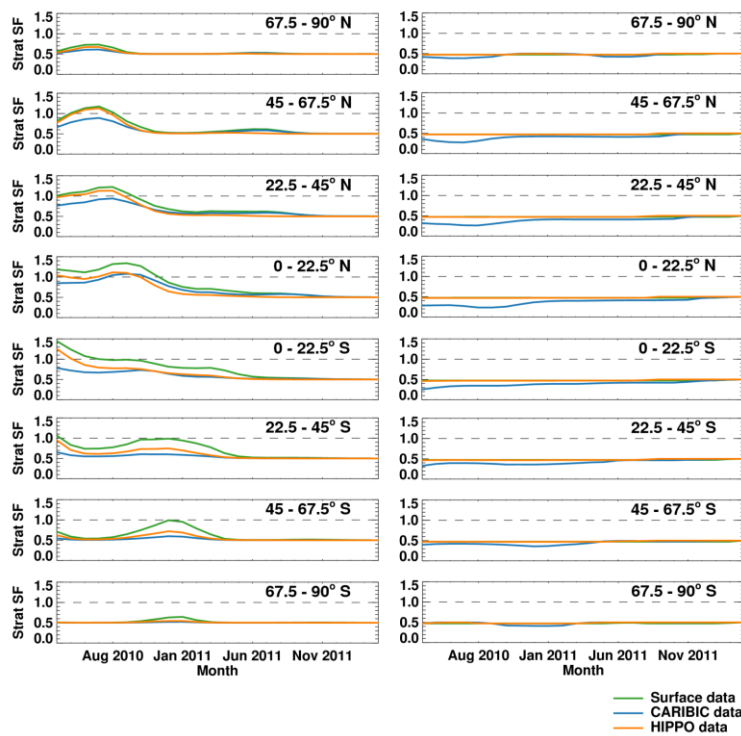
Figure 6. Pseudo observation tests optimizing N_2O stratospheric loss frequencies. Shown are a posteriori scaling factors (SF) for stratospheric loss frequencies in each of eight equal latitude bands for pseudo observation tests in which we optimize solely the stratospheric loss frequencies (left panels) or the emissions and stratospheric loss frequencies jointly (right panels). The latitude range of each band is indicated in the upper right hand corner of each panel. The true model value (1.0) is indicated by the black dashed line; each test started with a priori SF of 0.5 for each latitude band. Results obtained using surface data, CARIBIC data, and HIPPO data are shown in green, blue, and yellow, respectively.

1
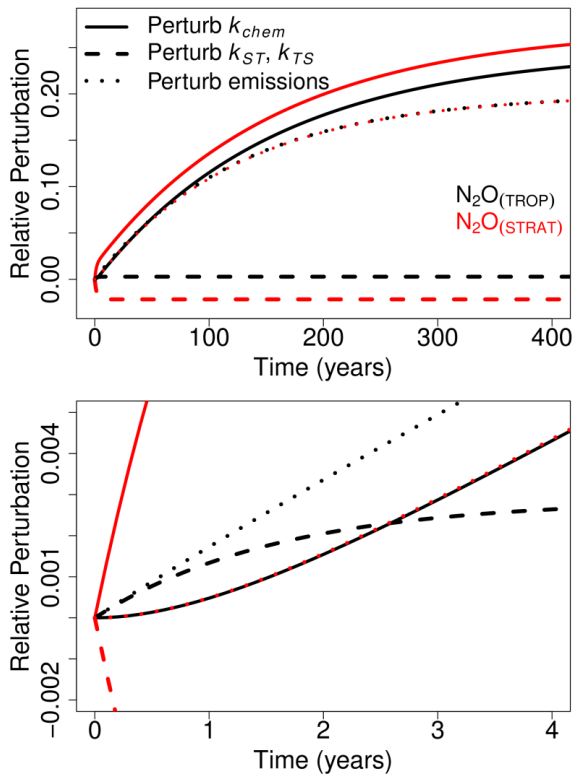
Figure 7. Results from a 2-box model illustrating the sensitivity of the tropospheric N_2O burden (and hence source inversions) to the N_2O stratospheric loss rate and to the rate of stratosphere-troposphere exchange. Shown are the relative perturbations to the tropospheric (black lines) and stratospheric (red lines) N_2O burdens resulting from: a 20% change in the N_2O stratospheric loss frequency (Perturb k_{chem}, solid lines); a 20% change in the rate of stratosphere-troposphere exchange (Perturb k_{ST}, and k_{TS}, dashed lines); and a 20% change in emissions (Perturb emissions, dotted lines). The top panel shows results over a 400-year timescale, while the bottom panel shows the initial 4 years.
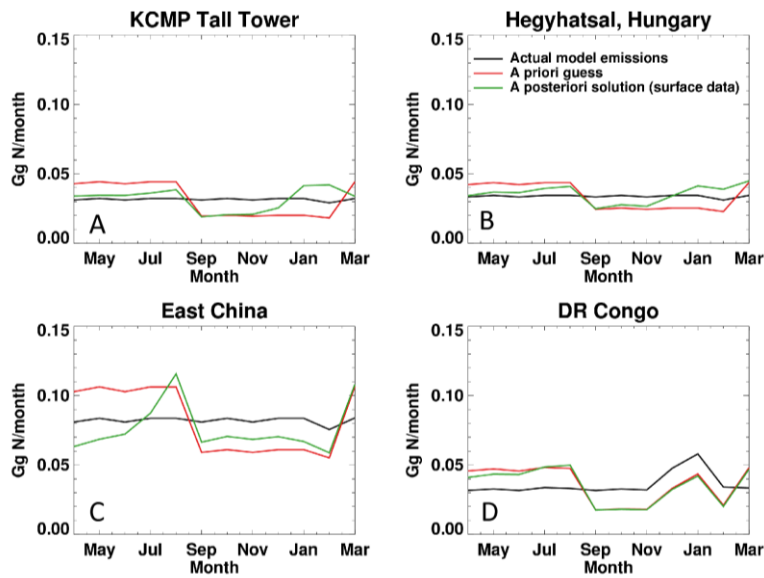
Figure 8. Resolving seasonal emission biases. The panels show the results from an OSSE in which a seasonally-dependent a priori emission bias is applied and we test the ability of the inversion to recover the true model fluxes. Results are shown for a site with continuous observations (KCMP Tall Tower), a site with ~weekly flask observations (Hegyhátsál, Hungary), a site with routine flask measurements ~1000 km downwind (East China), and a remote site in the Democratic Republic of Congo (DR Congo). The a priori (red), a posteriori (green) and true model fluxes (black) are plotted for the first year of the simulation (April 2010 – March 2011), with the a priori guess for soil emissions biased high in the first half of the inversion period (1.5×; March – August) and biased low in the second half (0.5×; September – February).

201004 Surface Error Reduction

201004 CARIBIC Error Reduction

201105 HIPPO Error Reduction

201108 HIPPO Error Reduction
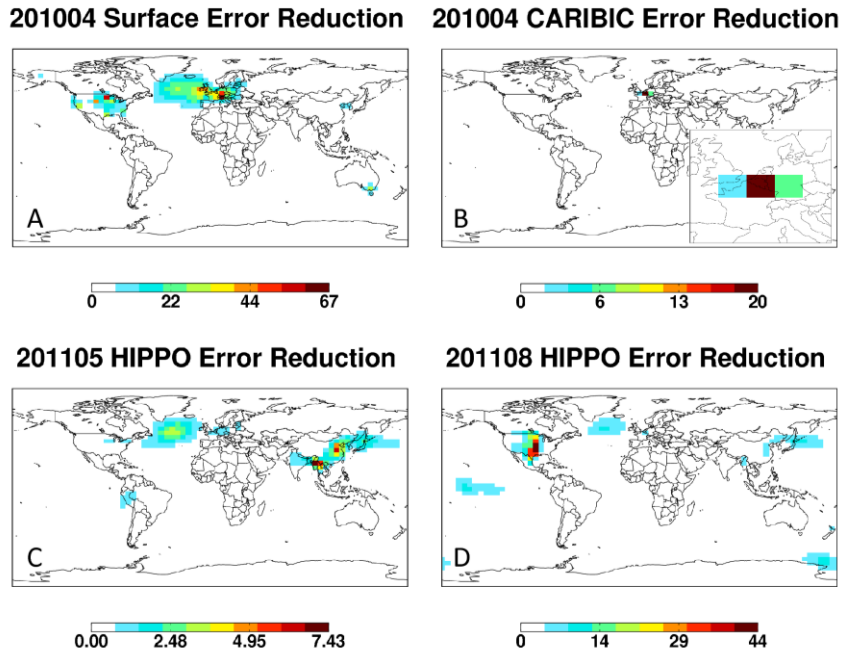
Figure 9. Error reduction (%) in N_2O emissions achievable in selected months using surface (A), CARIBIC (B), and HIPPO (C and D) measurements. An inset shows regional detail for the CARIBIC results. The relative error reduction is calculated based on a stochastic estimate of the inverse Hessian of the cost function for the inversion, and represents the ability of the observing system to remove a random emission error for each given location in the absence of any large-scale source bias.

201004 KCMP Avg Kernel

-0.01 0.29 0.59 0.90

201004 Hegyhatsal Avg Kernel

-0.03 0.08 0.18 0.28

201004 East China Avg Kernel

-4.90e-03 6.58e-03 1.81e-02 2.95e-02

201004 DR Congo Avg Kernel

-1.15e-03 2.68e-04 1.69e-03 3.11e-03
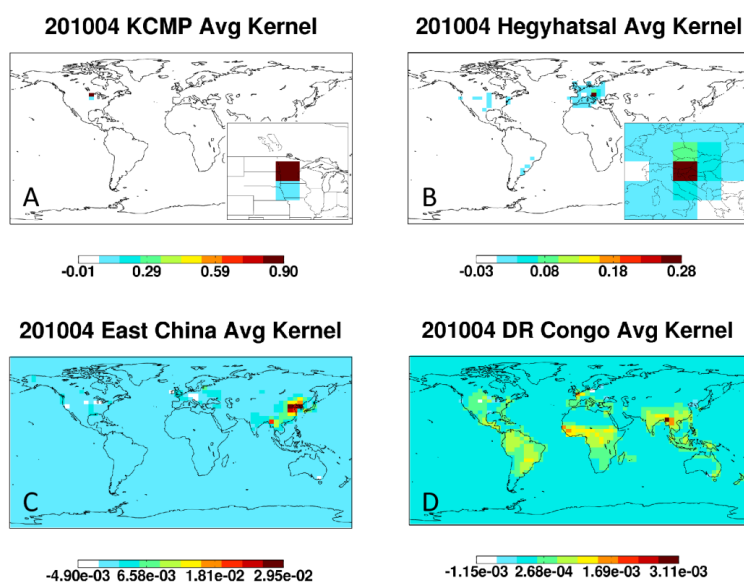
Figure 10. Rows of the averaging kernel for the inversion of N$_2$O emissions based on surface observations. The results indicate how well emissions in a particular location can be resolved from emissions elsewhere, and are shown for four example sites: (A) KCMP tall tower, (B) Hegyhátsál, Hungary, (C) a grid cell in East China, and (D) a grid cell in the Democratic Republic of Congo. Insets show regional detail for the first two sites. KCMP is a site with continuous observations, Hegyhátsál is a site with ~weekly flask observations, the East China site is a location with flask observations ~1000 km downwind, and the Congo site is a remote location.
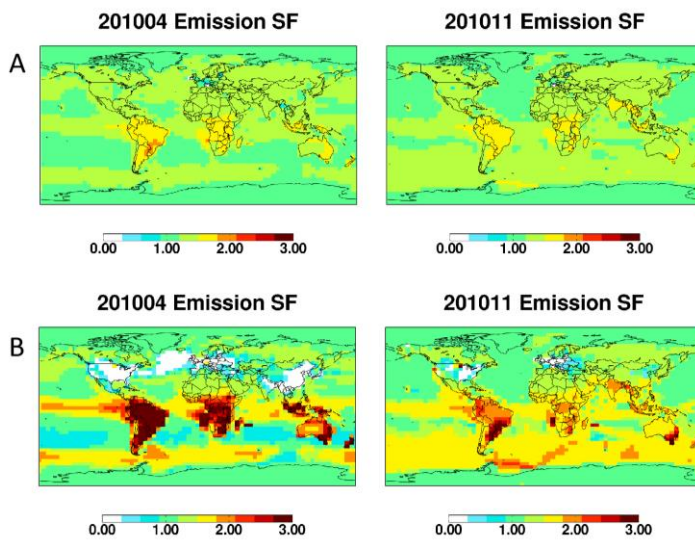
Figure 11. Inversion of N$_2$O emissions based on real surface observations. A posteriori emission scaling factors are shown for two different prior error assumptions: (A) 100% a priori error and horizontal covariance length scales of 500 and 1000 km for land and ocean emissions, respectively; and (B) no penalty term in the cost function.
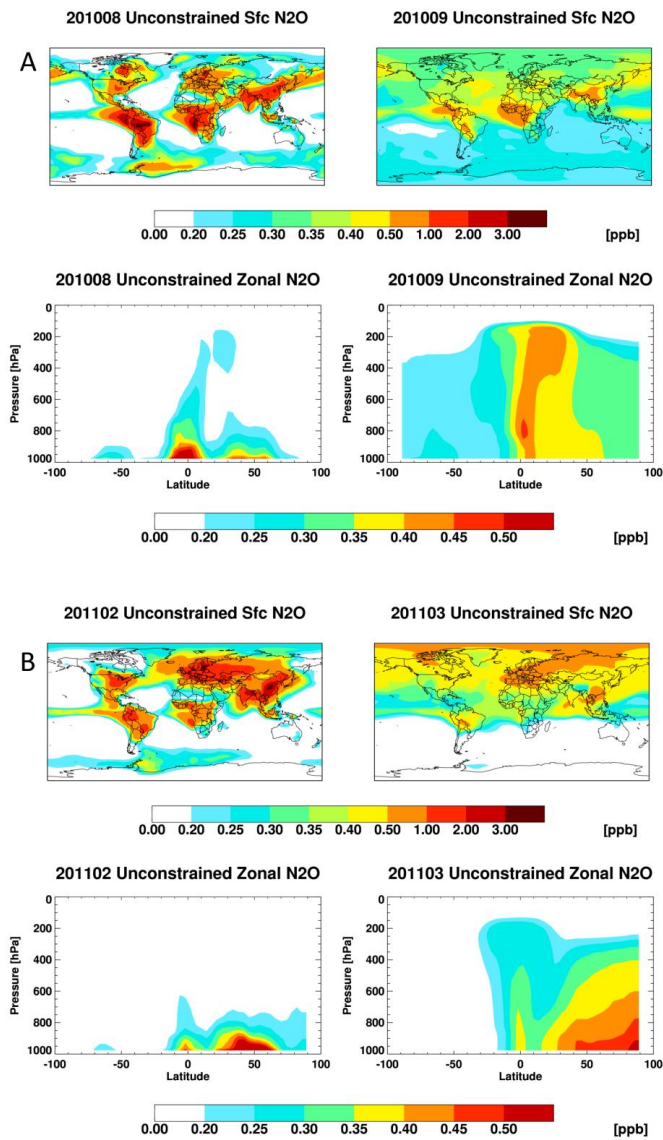
Figure 12. Distribution of unconstrained N_2O simulated by GEOS-Chem during the month of emission (August 2010 and February 2011) and the subsequent month. Unconstrained concentrations are calculated by scaling emissions for a particular month by $(1 - x)$, where x is the map of emission error reductions achieved using surface observations of N_2O. The initial atmospheric burden of N_2O and the emissions in the ensuing months are set to zero in order to highlight the spatial dispersal of unconstrained N_2O. Note nonlinear color scales.